THESIS

OBSERVATIONS OF ACYL PEROXY NITRATES DURING THE FRONT RANGE AIR POLLUTION AND PHOTOCHEMISTRY ÉXPERIMENT (FRAPPÉ)

Submitted by

Jake Zaragoza

Department of Atmospheric Science

In partial fulfillment of the requirements

For the Degree of Master of Science

Colorado State University

Fort Collins, Colorado

Spring 2016

Master's Committee:

Advisor: Emily V. Fischer

Jeffrey L. Collett, Jr.
Delphine Farmer

ABSTRACT

OBSERVATIONS OF ACYL PEROXY NITRATES DURING THE FRONT RANGE AIR POLLUTION AND PHOTOCHEMISTRY ÉXPERIMENT (FRAPPÉ)

The Colorado Front Range is an ozone (O_3) nonattainment region. The photochemistry of the region is influenced by emissions from the urban and oil and gas sectors, the complex terrain, and the meteorology. The Front Range Air Pollution and Photochemistry Éxperiment (FRAPPÉ) was a field intensive carried out in the Colorado Front Range during summer 2014 to characterize the regional chemical environment. Acyl peroxy nitrates (PANs) play important roles in atmospheric chemistry, acting as either sinks or sources for nitrogen oxides (NO_x) depending on conditions. PANs and other trace gas species were measured at the Boulder Atmospheric Observatory (BAO) during FRAPPÉ. Situated at the southwestern edge of the Denver-Julesburg Basin and 35 km north of Denver, BAO has been the site of multiple field studies aiming to characterize the influence of emissions from the oil and gas sector.

Here we focus on an analysis of the PANs measurements from BAO during FRAPPÉ. In particular, we focus on peroxyacetic nitric anhydride (PAN, $CH_3C(O)O_2NO_2$), peroxymethacrylic nitric anhydride (MPAN, $CH_2C(CH_3)C(O)O_2NO_2$) and peroxypropionic nitric anhydride (PPN, $CH_3CH_2C(O)O_2NO_2$). Mean and maximum PAN mixing ratios (5-minute point) were 275 and 1519 pptv respectively. There were four days during FRAPPÉ where the observed PAN abundance exceeded 1 ppbv. These days were examined using FLEXible PARTicle dispersion model (FLEXPART) back trajectories in order to determine air mass origin. The high PAN days occurred when air masses were recirculating in the region, often under Denver

Cyclones. However, a visual inspection of FLEXPART trajectories throughout FRAPPÉ showed that recirculation events in the region occurred on days with high (>1 ppbv), moderate (500 pptv − 1 ppbv), and low (<500 pptv) afternoon PAN mixing ratios.

The PPN/PAN ratio observed at the BAO tower during the summer of 2014 was 21%, which suggests anthropogenically enhanced photochemical activity. The ratio was very consistent (R^2 = 92%) and not dependent on wind direction, potentially reflecting a lack of variability in regional non-methane volatile organic compound (NMVOC) chemistry. The MPAN/PAN ratio was <5%, indicating that isoprene oxidation had very little influence on photochemistry compared to many other regions in the U.S. The relative abundances of PPN and MPAN were used to estimate the contribution of isoprene oxidation to local O_3 production. It was found that the contribution to local O_3 from isoprene oxidation was consistently less than 20%. The findings of this study suggest that anthropogenic emissions are the key drivers of PANs and O_3 formation in the region.

ACKNOWLEDGEMENTS

First and foremost I would like to thank my parents. Even though they have had no idea what I have been doing these past few years, they have provided their unconditional support, love, and the occasional care package to keep me motivated and keep me grounded. Los quiero mucho! I would like to thank my advisor, Dr. Emily Fischer, for always finding ways to excite the scientist in me. I would like to acknowledge anyone who has helped me with my thesis, whether through field site logistics, coding, model runs, or provision of data, countless individuals have helped me make this thesis possible. I would like to acknowledge my funding agencies, the SOARS Program, CSU's AGEP program, and the Colorado Department of Public Health and Environment for providing the funding that allowed me to participate in the FRAPPÉ study. Finally, and most importantly, I would like to thank all of the friends I made here in Fort Collins. You guys and gals kept me sane, Thank You!

TABLE OF CONTENTS

Chapter 1: Introduction

Most of the population of Colorado lives in the Northern Front Range Metropolitan Area (NFRMA), encompassing the cities of Denver, Boulder, Longmont, Greeley, and Fort Collins. This region has experienced some of the largest population growth in the state, with positive percent changes in population ranging from 11.2% in Denver County (http://quickfacts.census.gov/qfd/states/08/08031.html) to 4.5% in Jefferson County (http://quickfacts.census.gov/qfd/states/08/08059.html) between 2010 and 2014. The NFRMA is currently an ozone (O_3) nonattainment area. O_3 is a known respiratory irritant that can exacerbate asthma [*Thurston et al.*, 1997] and has been linked to increased risks of death via respiratory causes [*Jerrett et al.*, 2009]. Regional O_3 exceedances occur despite evidence of decreases in nitrogen oxides ($NO_x = NO + NO_2$) in the NFRMA [*Cooper et al.*, 2012; *Russell et al.*, 2012]; *Russell et al.* [2012] found a -4.05% yr^{-1} change in the NO_2 column over Denver between 2005 and 2011, although the total reduction was less than a standard deviation of the mean reduction for all cities studied. The photochemistry in the NFRMA responds to many factors, some of which are unique to the region, and some of which are emblematic of issues facing broad swaths of the western U.S. [*Brodin et al.*, 2010].

Unconventional fossil fuel extraction in Colorado is increasing and emissions are poorly constrained [*Gilman et al.*, 2013; *Pétron et al.*, 2012; *Swarthout et al.*, 2013; *Thompson et al.*, 2014]. Crude oil and natural gas production has increased in Colorado over the last decade, with increases of 146% between 2007 and 2013 for crude oil production and 38% for natural gas production between 2007 and 2012 (http://www.eia.gov/state/print.cfm?sid=CO). Colorado is

also in the top ten states for total energy production (http://www.eia.gov/state/rankings/?sid=CO#/101). Weld County, situated north-northeast of Denver, is the largest producer of oil and natural gas in Colorado. As of January 2015, this region accounted for almost 90% of the oil and almost 30% of the natural gas (http://www.drillingedge.com/colorado/wells) produced within the state. Oil and gas production in the area accounts for approximately 75% of CH_4 emissions in the region [*Pétron et al.*, 2014], and between a quarter to more than half of the volatile organic compound (VOC)-OH reactivity in the region has been attributed to emissions from this sector [*Gilman et al.*, 2013; *Swarthout et al.*, 2013].

There are also a number of other relevant issues for western U.S. regional air quality. Briefly, evidence exists for direct O_3 transport into the U.S. from the west [*Cooper et al.*, 2012; *Cooper et al.*, 2010; *Parrish et al.*, 2009]. The summer fire season appears to be increasing in severity and duration [*Westerling et al.*, 2006], and summertime temperatures in Colorado are rising [*Cooper et al.*, 2012]. Hence, predicting O_3 in the NFRMA is difficult because of the combined effects of complex sources, circulation, and terrain.

The acyl peroxy nitrates (PANs) are secondary species formed in the same complex photochemical environment that forms O_3 [*Singh and Hanst*, 1981]. The PANs also constitute a significant portion of the total reactive nitrogen budget (NO_y) [*Roberts et al.*, 2004; *Singh*, 1987; *Singh et al.*, 1994; *Singh et al.*, 1985]. PAN ($CH_3C(O)O_2NO_2$) is the most abundant member of the PANs family. A suite of both biogenic and anthropogenic VOC precursors can contribute to PAN formation, and the main oxidation intermediates are acetaldehyde, acetone, and

methylglyoxal [*Fischer et al.*, 2014]. Other abundant members of the PANs family have different organic intermediate species that can be attributed to specific emitted precursors. Thus, the relative abundance of different PAN homologues can be used to diagnose the types of VOCs that are photochemically important in a region [*Roberts et al.*, 2003; *Roberts et al.*, 1998; *Williams et al.*, 1997].

One goal of the Front Range Air Pollution and Photochemistry Éxperiment (FRAPPÉ) field intensive (9 July - 22 August 2014) was to constrain the emissions of O_3 precursors and formation rates in the NFRMA. The campaign was simultaneous with the final phase of the NASA DISCOVER-AQ mission (http://discover-aq.larc.nasa.gov/). In this study, we present measurements of the PANs and O_3 from a ground site.

Chapter 2: Methods

2.1 Site Description

The Boulder Atmospheric Observatory (BAO) (40°N, 105°W, 1584 m ASL) was one of the major supporting ground-based sites that housed a large suite of trace gas and aerosol measurements during FRAPPÉ (Figure 1). Recent winter (2011) [*Gilman et al.*, 2013; *Swarthout et al.*, 2013] and multi-year (2007-2010) [*Pétron et al.*, 2012] measurements from BAO have explored the impacts of VOC emissions from oil and natural gas operations on trace gas composition in the Colorado Front Range. BAO has a 300 m tower outfitted with a suite of meteorological instrumentation at 3 different levels (10, 100, 300 m AGL) [*Hahn*, 1981; *Kaimal and Gaynor*, 1983]. In this analysis we use wind speed and direction measured at 10 m. During the FRAPPÉ field intensive, instruments were housed in either a vertically mobile carriage mounted on the south-southwest face of the BAO tower [*Brown et al.*, 2013], or a trailer parked at the base of the tower. The PAN instrument was located in the trailer at the base of the tower (Figure 2). The carriage, known as the Profiling Instrument Shelter with Amenities (PISA) was used for both vertical profiling and stationary measurements [*Brown et al.*, 2013]. For FRAPPÉ, the PISA sheltered several instruments including a Picarro G2401 cavity ring-down instrument for the measurement of CO, CO_2, and CH_4 and the Atmospheric Ring-down Nitrogen Oxide Laser Detector (ARNOLD) for the measurement of N_2O_5, NO_2, NO, O_3, and NO_y ($NO + NO_2 + NO_3 + 2N_2O_5 + HNO_3 + HONO + HO_2NO_2 +$ PANs + aerosol nitrates + organic nitrates + …) [*Dubé et al.*, 2006; *Fuchs et al.*, 2008]. PAN measurements were made from 9 July to 22 August 2014.

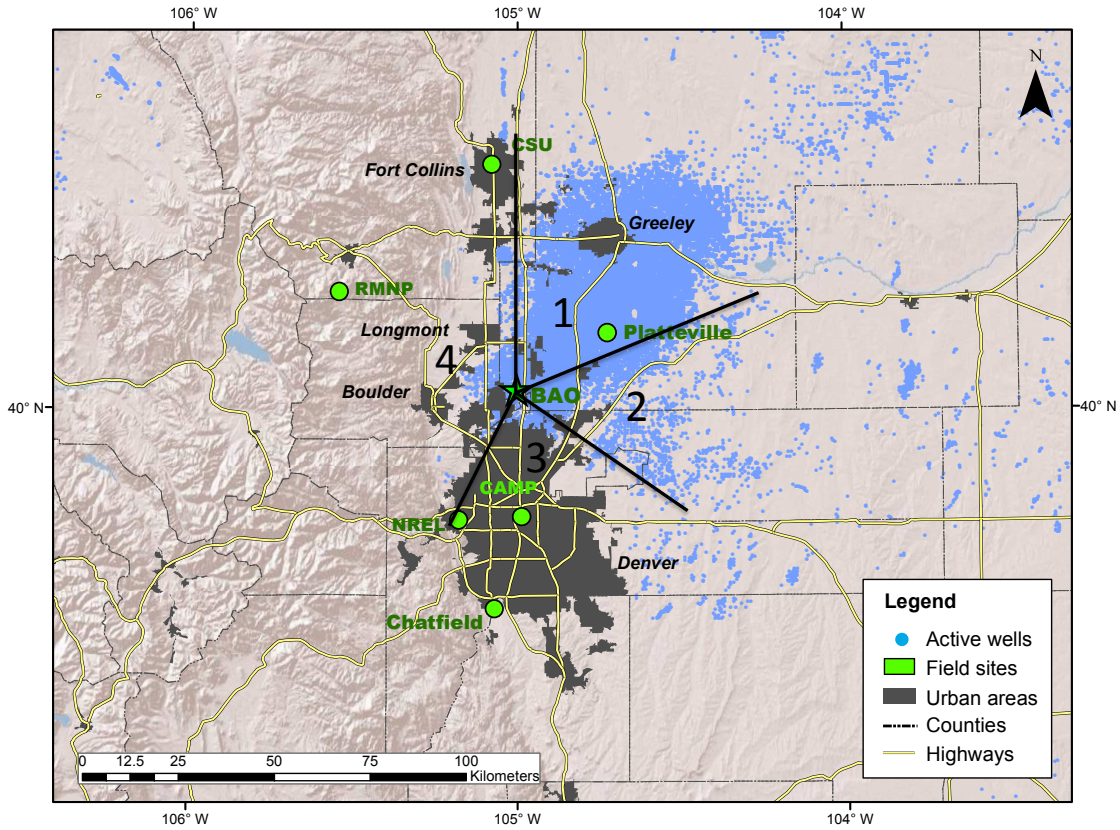

Figure 1: Map of region with the location of major FRAPPÉ sites (green), oil and gas wells (blue), highways (yellow), and major urban areas (grey). The solid black lines represent the boundaries for the FLEXible PARTicle dispersion model (FLEXPART) sector analysis (Chapter 3).

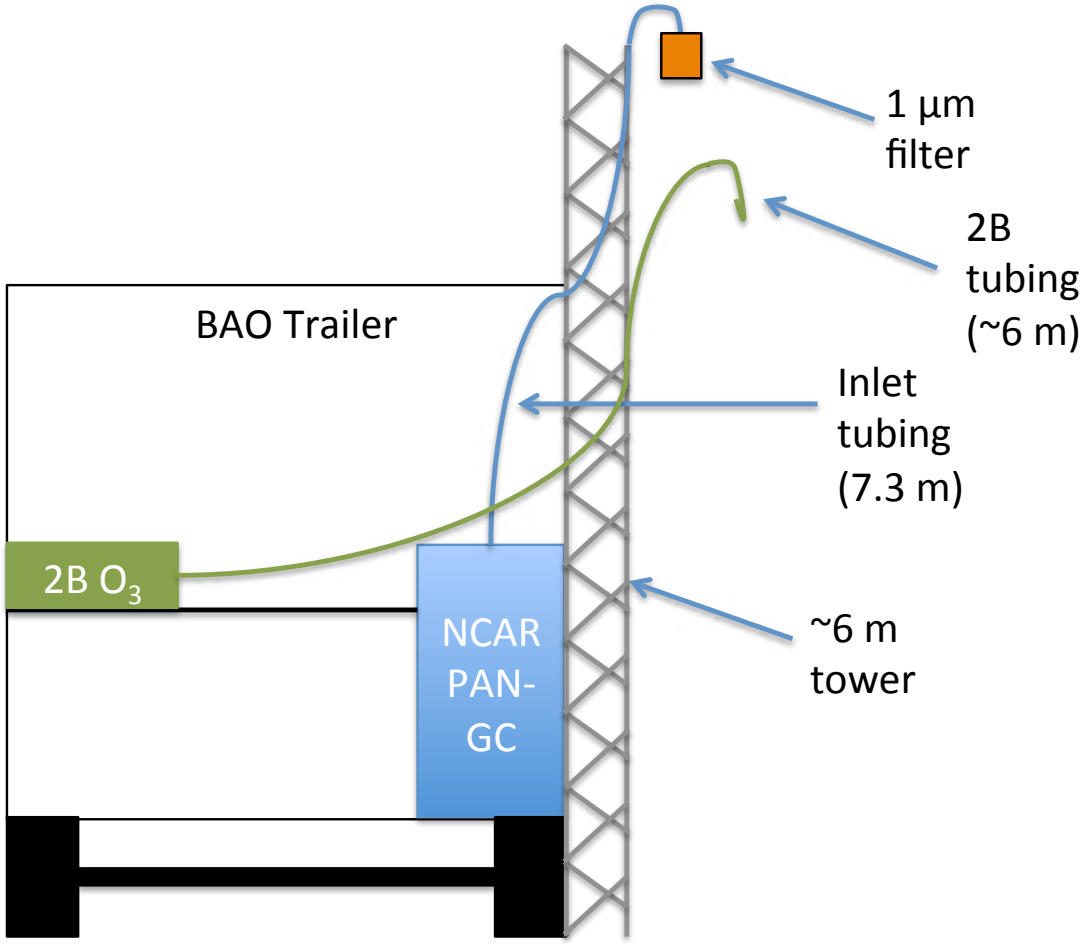

Figure 2: Ground-based trailer setup during FRAPPÉ. The 2B Technologies Ozone Monitor and the National Center for Atmospheric Research (NCAR) PAN gas chromatograph (NCAR PAN-GC) were both housed in this trailer. Inlets were attached to the 6 m scaffolding.

2.2 PAN Measurements

PANs were measured with the NCAR gas chromatograph with an electron capture detector (GC-ECD) [*Flocke et al.*, 2005]. The NCAR PAN GC-ECD is a dual channel system with a common sampling loop and ECD. A full description of the instrument can be found in *Flocke et al.,* [2005] (see Appendix for plumbing diagram). For this campaign, the NCAR PAN GC-ECD was configured to collect a point sample every five-minutes. The sampling inlet was located at a height of ~6 m on a scaffolding erected above the trailer (Figure 2). PAN was

sampled through a 0.635 cm (1/4 inch) external diameter, 0.476 cm (3/16 inch) internal diameter, Teflon line (Fisher Scientific Part Number: NCO171958) with a 1 μm Teflon filter (Savillex Part Number: 401-21-47-10-21-2) located at the inlet. Flow through the 7.3 m long line was approximately 7 LPM, yielding a residence time of less than a second in the main inlet. At 27°C with an assumed afternoon average NO_2 to NO ratio of 4, the lifetime of PAN is ~2.7 hours. The instrument sampled off this main line at a slower flow rate (~50 mL/min).

Automated point calibrations were performed throughout the campaign at 4-hour intervals, with more frequent calibrations during the initial week of the campaign. Point calibrations were augmented by multi-point calibrations mid-campaign (see Appendix for point and multi-point calibrations). PAN for calibrations was generated using a continuous-flow acetone photolysis cell [*Warneck and Zerbach*, 1992]. Briefly, peroxyacetyl radicals were generated by the photolysis (254 nm lamp Jelight Part Number: 84-285-2) of 20 ppmv acetone in ultra-zero air (Scott-Marrin Tank Number: CB10757) in the presence of O_2. An accurately measured flow of NO (1 ppmv NO in N_2, Scott-Marrin Tank Number: CB10671) was added to the gas stream. A zero-air generator was used as a dilution source. The calibrator efficiency was assumed to be 93% for the conversion of NO to PAN [*Volz-Thomas*, 2002].

We estimated the uncertainty of the PAN mixing ratio produced by the calibrator to be 9%, and this was calculated as the root sum of squares of the error in all the calibration components. This includes the calibration gases (5% for acetone and 2% for NO), gas flow controllers (1% for acetone, 3% for NO, and 6% for the zero-air generator), and the calibrator efficiency (3%) [*Volz-Thomas*, 2002]. Halfway through the campaign, the chromatograms began

experiencing “noisy” baselines as a result of an unknown electrical noise source (see Appendix for example chromatograms). This resulted in separate precision and limit of detection calculations for “clean” and “noisy” baselines. The precision of the system was determined by calculating the relative standard deviation of PAN peak areas for campaign-wide point calibrations in both columns, for the “clean” and “noisy” baselines, resulting in four different precision calculations (6% and 4% for PAN on columns 1 and 2, respectively, for “clean” baselines and 3% for PAN on both columns for “noisy” baselines). The uncertainty was estimated as the root sum of squares of the uncertainty of the calibrator and the precision of the point calibrations, resulting in four different uncertainties (11% and 10% for PAN in columns 1 and 2, respectively, for “clean” baselines and 10% for PAN on both columns for “noisy” baselines). The precision and uncertainty values on the “noisy” baselines are lower because we increased the sample pressure to create larger peak areas. The limits of detection (LOD) were calculated as three times the standard deviation of the baseline during example “clean” and “noisy” periods. The LODs were approximately 2 pptv for “clean” chromatograms and 20 pptv for “noisy” chromatograms (see Appendix for uncertainty and LOD calculations).

The other PANs members used in this analysis, peroxymethacrylic nitric anhydride (MPAN, $CH_2C(CH_3)C(O)O_2NO_2$) and peroxypropionic nitric anhydride (PPN, $CH_3CH_2C(O)O_2NO_2$), were not directly calibrated. Instead, their mixing ratios were obtained as response factors relative to PAN. The PPN and MPAN response factors are 0.90 ± 0.02 and 0.64 ± 0.03, respectively. See *Flocke et al.* [2005] for more information about how the response factors were obtained.

2.3 Supporting Measurements

Measurements of CO, CO_2, and CH_4 were made using a four channel Picarro Cavity Ring-Down Spectrometer (CRDS, Picarro Model G2401). We performed water tests for the analyzer prior to the campaign following *Chen et al.* [2013]. During FRAPPÉ, a short inlet (~1 m) associated with the Picarro was located on the bottom of the PISA carriage, and air was sampled through an in-line 7 μm filter. Five NOAA standard reference gases (http://www.esrl.noaa.gov/gmd/ccl/refgas.html) were used for calibrations. Two standard reference gas mixtures (JA02336 and JB03049) were used as field calibration standards during the campaign at 3-hour intervals and three standard reference gas mixtures (CA06969, CB10166, and CA08244) were used to perform laboratory instrument calibrations, pre- and post-campaign.

The ARNOLD, a NOAA custom-built CRDS, was used to make measurements of N_2O_5, NO_2, NO, O_3 and NO_y based on the in-situ detection of NO_2 and NO_3 during FRAPPÉ [*Brown et al.*, 2002]. Specific instrument details have been described previously [*Brown et al.*, 2002; *Dubé et al.*, 2006; *Fuchs et al.*, 2009; *Washenfelder et al.*, 2011; *Wild et al.*, 2014]. Briefly, N_2O_5 is thermally dissociated to NO_3, which is directly detected at 662 nm [*Dubé et al.*, 2006]. NO_2 and the remaining species are measured via the detection of NO_2 at 405 nm [*Fuchs et al.*, 2009; *Washenfelder et al.*, 2011; *Wild et al.*, 2014]. NO and O_3 are chemically converted to NO_2 [*Fuchs et al.*, 2009; *Washenfelder et al.*, 2011], while NO_y is thermally reduced using a quartz heater (650°C) and subsequently converted to NO_2 via a small addition of O_3 [*Wild et al.*, 2014].

O_3 was also measured in the ground-based trailer (Figure 2) with a 2B Technologies Model 202 Ozone Monitor. The 0.635 cm Teflon inlet was located at a height of 5.08 m and

pulled through ~6 m of tubing at approximately 1 LPM. The Model 202 was calibrated before, once during, and after the campaign with a 2B Technologies Model 306 Ozone Calibration source.

2.4 Description of FLEXPART model

FLEXPART is a Lagrangian particle dispersion model used to simulate atmospheric transport and dispersion [*Stohl et al.*, 2005]. For this application, a version of FLEXPART was used that was coupled to the Weather Research and Forecasting (WRF) model (http://www.wrf-model.org) as described by *Brioude et al.* [2013]. WRF was set up using a 3 km horizontal resolution over the domain of Colorado and adjacent states. For FRAPPÉ, FLEXPART was run forward in time to understand the dispersion of different emissions sources and backward to understand the history of an air mass impacting a site, BAO in this case. In the case of the backward runs, 100,000 particles – representing inert air tracers – were released during the first hour at each release point (*e.g.* BAO) randomly between 0 and 100 m AGL, and followed backwards in time for 24 hours. At each hour, the spatial distribution of particles in the lowest 100 m was multiplied with a gridded description of emission fluxes from various sources. The sum over all grid cells of the result for each source category was plotted as stacked bars on the right-hand plots in Figure 5. Thus, the stacked bars represent the contribution (over time) of each emission source, in arbitrary mass units, to the air measured at the release point during the time the particles were released. It should be noted that all source categories decayed at the same e-folding lifetime of 48 hours and the stacked bars have been scaled accordingly. In Figure 5 (left side) we additionally present the spatial distribution of particles used to calculate the above mentioned stacked bars, color-coded by the hours since release.

Fire emissions are based on the Fire Inventory from NCAR (FINN) [*Wiedinmyer et al.*, 2011]. Emissions of isoprene and lumped monoterpenes are based on the Model of Emissions of Gases and Aerosols from Nature (MEGAN) [*Guenther et al.*, 2006]. The remaining categories are based on extracted sub-categories of the 2011 Environmental Protection Agency (EPA) National Emission Inventory (NEI), with "Out of CO" representing the total emissions of regions outside of Colorado. We used the following emitted species from the NEI for the different categories: NO_x (Mobile, Area/point, Out of CO), NH_3 (Agriculture), and ethane (Oil and Gas).

2.5 Standard Major Axis Regression (Reduced Major Axis Regression)

Typically for linear regressions, the independent variable (x) is set and the dependent variable (y) is measured. The equation for a line resulting from the regression can then be used to describe the relationship between the two variables or to predict the response of the dependent variable. Standard linear regression minimizes the sum of the squared deviations in the y-direction. In cases where neither variable can be controlled, an ordinary least squares regression will tend to underestimate the slope. Standard major axis (SMA) regression, also known as reduced major axis (RMA) regression, is a regression technique used when the two variables in the regression have error associated with them. Briefly, SMA minimizes the product of both the x and y deviations from the fitted line [*Ayers*, 2001]. We used RMA to determine the relationship between PPN, PAN and MPAN in Chapter 3 because all the measurements have error associated with them.

Chapter 3: Results & Discussion

3.1 Overview of Chemical Measurements

Figure 3 presents a time series of the 5-minute PAN data for the FRAPPÉ campaign. Similar to observations at other ground sites [*E Grosjean et al.*, 2001; *Ridley et al.*, 1990; *Roberts et al.*, 2003; *Roberts et al.*, 1998], PAN shows a pronounced diurnal cycle at BAO, likely reflecting daytime photochemical production and nighttime deposition. Daytime hourly PAN was positively correlated with NO_z (NO_y - NO_x) throughout the campaign, with an average PAN/NO_z ratio of 0.14 (see Appendix for PAN/NO_z plot). PAN mixing ratios greater than 1 ppbv were observed on 4 days: 15, 23, 29 July and 19 August. These days are labeled in Figure 3. PAN was also measured on the C-130 research aircraft (with a thermal dissociation chemical ionization mass spectrometer (TD-CIMS)) [*Zheng et al.*, 2011] and at a ground site in Rocky Mountain National Park (RMNP, 40.3°N, 105.5°W, 2743 m ASL, via GC-ECD) during the FRAPPÉ campaign [*Callahan et al.*, 2014]. For comparison with the BAO PAN data, we confined data from the C-130 to approximately 40 – 41°N and 104 – 105°W below 3 km. Only one out of the four days with afternoon PAN mixing ratios greater than 1 ppbv occurred during a C-130 research flight day in the region (red shading in Figure 3). In general, the C-130 average is expected to be higher because: 1) C-130 flights were made during the day, usually in the afternoon, where photochemistry is assumed to be most active; and 2) C-130 flights were above the surface, where the temperature is cooler and the lifetime of PAN, with respect to thermal decomposition, is expected to be longer. The air mass histories associated with these elevated BAO PAN events are discussed in section 3.2. As a result of the "noisy" baselines in August on the NCAR PAN GC, MPAN mixing ratios were only quantified for July. Table 1 presents mean,

median, and maximum PAN, PPN, and MPAN mixing ratios, Figure 4 gives a box and whisker representation of the PANs measured during FRAPPÉ.

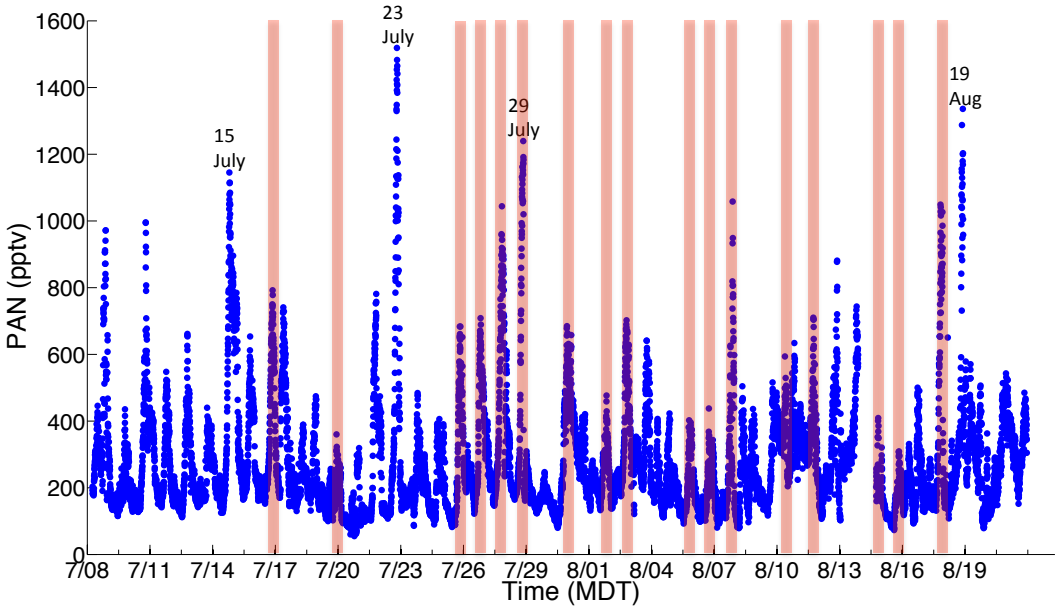

Figure 3: Time series of 5-minute point PAN mixing ratios. Peaks with marked days are examined below. Reddish bars signify C-130 flight days.

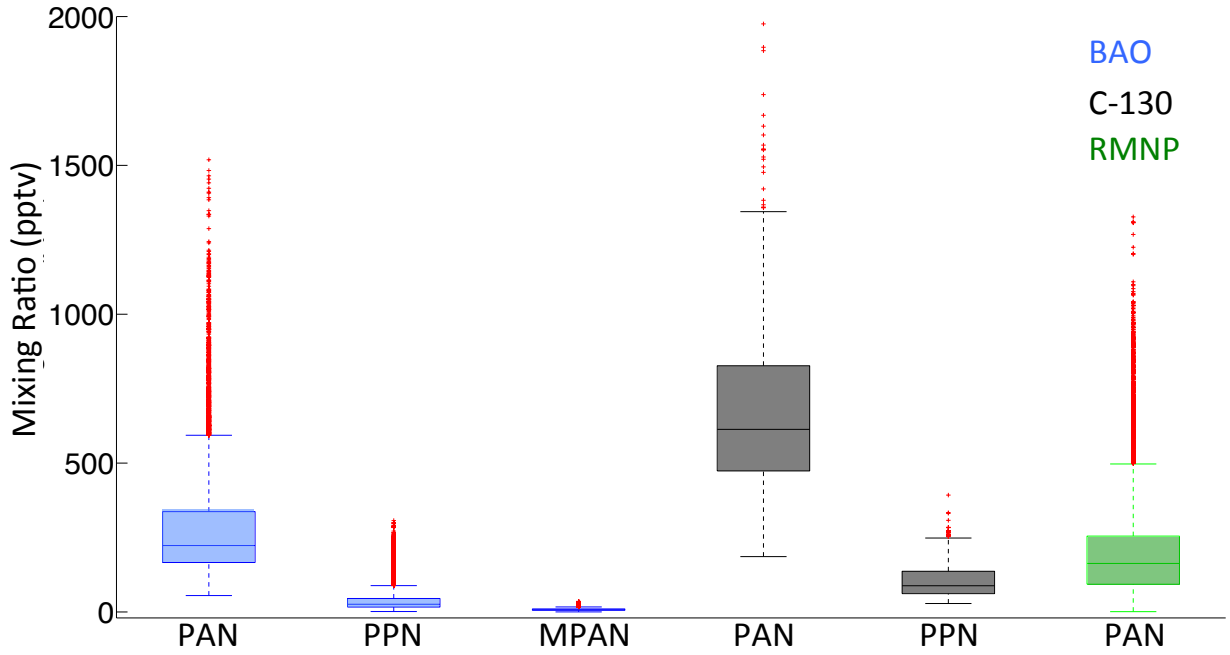

Figure 4: Box and whisker plots of PANs measured during FRAPPÉ from multiple platforms. The box represents the 25th percentiles, medians, and 75th percentiles. The whiskers represent the minimum and 95th percentiles, and the red x's represent individual observations above the 95th percentile. Data is given in Table 1.

Table 1: Mean, median, and maximum (with corresponding day) 5-minute point mixing ratios for PAN, PPN, and MPAN at BAO, (1-minute average mixing ratios) on the C-130 (40 – 41°N and 104 – 105°W below 3 km), and 5-minute point mixing ratios at RMNP during FRAPPÉ.

Site	PAN (pptv)			PPN (pptv)			MPAN (pptv)		
	Mean	Median	Max	Mean	Median	Max	Mean	Median	Max
BAO	275	223	1519 (23 July)	38	26	307 (23 July)	9	7	36 (29 July)
C-130	667	613	1975 (28 July)	106	88	393 (28 July)	N/A	N/A	N/A
RMNP	201	163	1327 (23 July)	N/A	N/A	N/A	N/A	N/A	N/A

3.2 Common Chemical and Meteorological Characteristics of Elevated PAN Plumes

In this section we focus our attention on afternoon periods with PAN mixing ratios greater than 1 ppbv. A description of the meteorological context combined with a discussion of

the FLEXPART results are used to identify common features in the air mass histories associated with each time period.

The Denver Cyclone is a mesoscale gyre that develops near the city of Denver, Colorado as a result of the mountainous terrain of the region [*Crook et al.*, 1990; *Szoke*, 1991; *Wilczak and Glendening*, 1988; *Wilczak and Christian*, 1990]. The gyre of winds can keep local emissions concentrated and recirculating over the region. Based on the data collected in summer 2014, a common feature of elevated PAN in the Front Range was the development of a Denver Cyclone. This mesoscale feature was present on 15, 23, and 29 July. Surface winds on 15 July indicated a pronounced cyclonic pattern that developed in the Front Range area. This circulation developed around 5 MDT and remained throughout the day, although after 8 MDT it was much less pronounced. Surface winds on 23 July also showed a very pronounced cyclonic pattern that developed around 3 MDT and also remained throughout the day before becoming less pronounced by 10 MDT. Finally, regional surface winds on 29 July indicate that cyclonic winds developed around 8 MDT and remained until about 15 MDT. The cyclonic winds characteristic of a Denver Cyclone were not clearly present on 19 August (see Appendix for regional winds).

The FLEXPART air mass histories presented in Figure 5 reflect recirculation of regional emissions. The 15 July (Figure 5a) air mass history highlights a very clear gyre-type path for an air mass with origins in eastern Colorado/western Kansas and Nebraska. The air mass loading plot for 15 July shows agricultural emissions impacting the air mass 9 – 3 hours before it arrived at BAO. Oil and gas emissions impacted the air mass during the 8 hours prior to arrival at BAO. The 23 and 29 July (Figures 5b and 5c, respectively) air mass histories both show air masses

lingering over the Front Range. The corresponding air mass loading plot for 23 July shows consistent biogenic VOC emissions, mobile, and area/point emissions impacting the air mass during the 12 hours before arrival at BAO, and oil and gas emissions impacting the air mass during the 2 hours before arrival at BAO. The air mass loading plot for 29 July shows consistent impact of emissions from biogenic VOC, oil and gas, mobile, area/point, and agriculture sources on the air mass during the 18 hours before arrival at BAO. Hence, on the high PAN days in July, evidence exists for air mass recirculation occurring in the Front Range area, with emissions from multiple sources influencing these air masses. The FLEXPART air mass history for 19 August (Figure 5d) does indicate some recirculation over the Front Range, even though regional winds did not show a cyclonic pattern. The corresponding air mass loading plot highlights an increase in emissions from multiple sources from about 12 hours before arrival onward.

On the high PAN days mentioned above, all air masses appear to travel over the Denver-Julesburg Basin (DJB) within hours of impact at the BAO site. Thus, based on the FLEXPART results we expect, and the data show, a positive relationship between PAN and CH_4 (Figure 6). As discussed in *Pétron et al.* [2014], there are other sources of CH_4 located to the northeast of BAO in addition to oil and gas activities. Beef and dairy production are major activities in Weld County, and there are also landfills and wastewater treatment facilities. However, *Pétron et al.* [2014] estimate that 75% of the total CH_4 emissions in this region can be attributed to oil and gas activities. Other more specific VOC tracers of oil and gas activity or specific PAN precursors, *e.g.* ethane, were not successfully measured at BAO during FRAPPÉ.

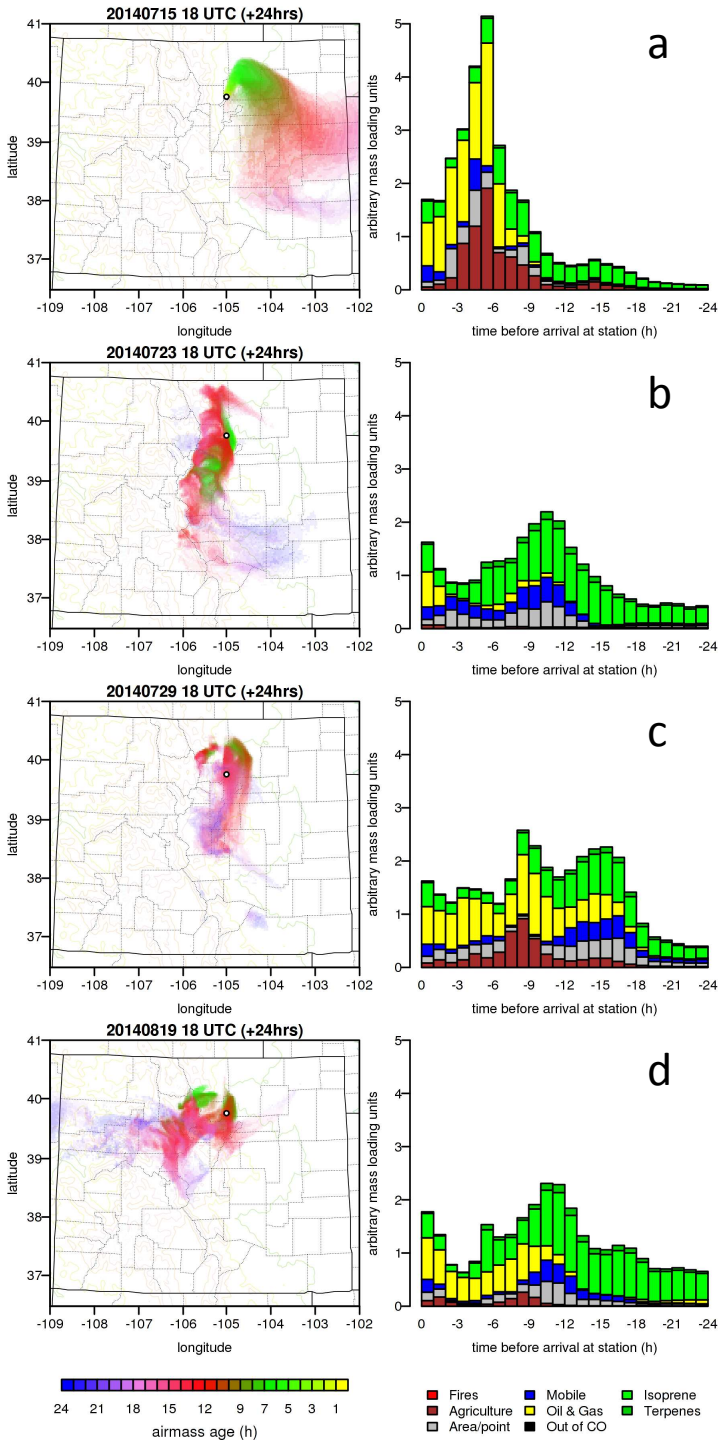

Figure 5: FLEXPART output for a) 15, b) 23, c) 29 July, and d) 19 August 2014. Left: 24-hour air mass histories for air impacting BAO between 11 am and 12 pm MDT. The circle represents the location of the BAO tower. Right: the contribution (over time) of various emission sources to the air mass.

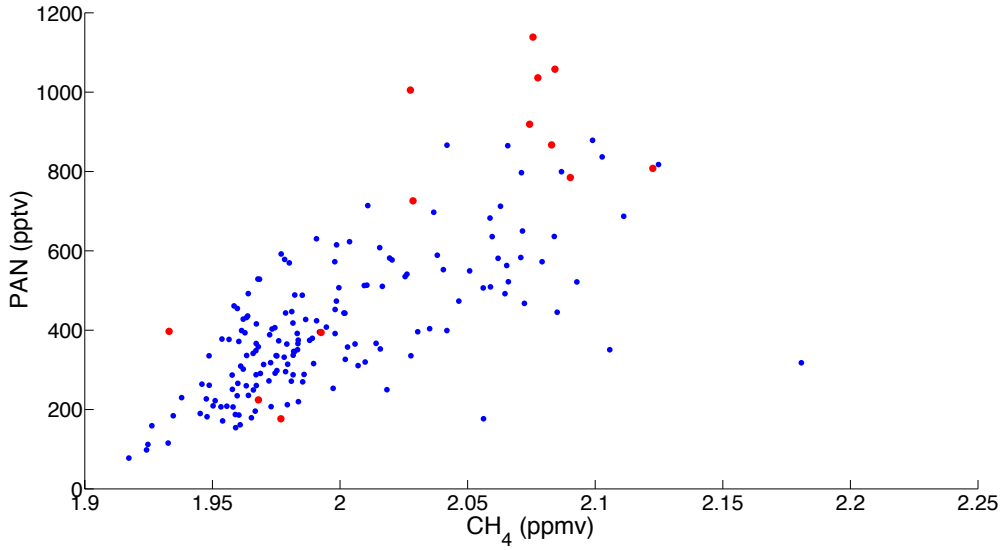

Figure 6: Relationship between hourly mean PAN and CH_4 at the BAO tower for afternoon periods (12 − 5 MDT) of the entire campaign. The red dots highlight days when peak PAN mixing ratios exceeded 1 ppbv.

3.2.1 FLEXPART Sector Analysis

Although the high PAN days were associated with recirculation in the area, recirculation type events were not exclusive to high PAN days. *Fischer et al.* [2006] classified air mass transport histories by source region based on the visual inspection of HYSPLIT and FLEXPART trajectories for the 2004 ICARTT field campaign. Similarly, a visual inspection of the FLEXPART back trajectories during FRAPPÉ was used to classify four major source regions for air masses impacting BAO. The BAO tower is located on the southwestern edge of the DJB and oil and gas development is prevalent all around the tower, but especially to the north-northeast (see Figure 1). This was defined as Sector 1 (S1), where emissions from oil and gas activities are expected to dominate the VOC emission profile, although emissions from agriculture are also significant [*Pétron et al.*, 2014]. Sector 2 (S2) encompasses the region between the southern edge of the DJB and the town of Bennett, CO (39.75°N 104.43°W). This sector is expected to

have a mix of emissions from agriculture as well as oil and gas activities. To the south of the BAO tower is Sector 3 (S3), an urban sector with large vehicle emissions defined to be between the southern edge of S2 and Golden, Colorado (39.75°N 105.21°W). Finally, Sector 4 (S4), the largest sector, is located between Interstate 25 and the western edge of Sector 3. The cities of Boulder, Longmont, and Fort Collins are located in this region. See Figure 1 for boundaries. The analysis was done for three PAN bins (low, mid, and high corresponding to <500, 500 − 1000, and >1000 pptv, respectively) and three times (6, 12, and 18 hours before).

Figure 7 highlights the results of the sector analysis, and Table 2 results as percentages. Across the PAN bins at 6 hours before arrival at the site, the air mass trajectories passed through at least 3 of the sectors at least 50% of the time. In the low PAN bin, the air mass trajectories passed through all 4 sectors at least 50% of the time. At 12 hours before arrival, across the PAN bins, the associated air mass trajectories passed through at least 2 of the sectors at least 50% of the time. In the high PAN bin, the air mass trajectories passed through all 4 sectors at least 50% of the time. At 18 hours before arrival, the air mass trajectories passed through Sector 4 at the highest frequency across the PAN bins. If we define recirculation as periods where the air mass trajectories travelled through multiple sectors within the same 24 hour period, then days with regional recirculation were not exclusive to days with PAN abundances >1 ppbv.

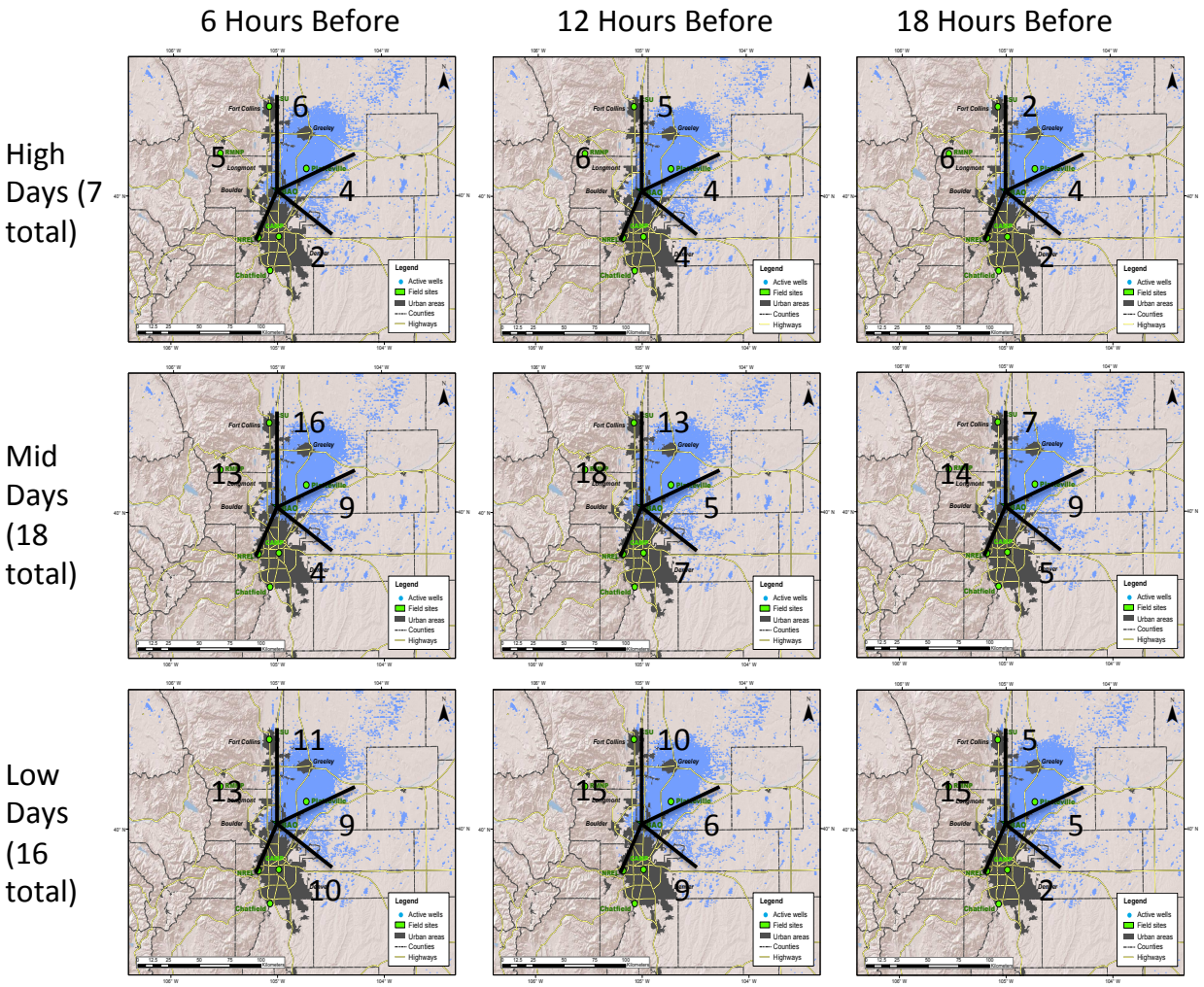

Figure 7: Results of the FLEXPART sector analysis. The number in each sector represents the number of times an air mass trajectory was found in the given sector, per PAN bin (High, Mid, and Low Days correspond to >1000 pptv, 1000 − 500 pptv, and <500 pptv, respectively) per time before impact.

Table 2: Results of the FLEXPART sector analysis. The values given represent the frequency (as a percentage) that an air mass trajectory passed through a given sector. See Figure 1 for the sectors.

	6 hours before				12 hours before				18 hours before			
	S1	S2	S3	S4	S1	S2	S3	S4	S1	S2	S3	S4
High PAN (7 days)	86	57	29	71	71	57	57	86	29	57	29	86
Mid PAN (18 days)	89	50	22	72	72	28	39	100	39	50	28	78
Low PAN (16 days)	69	56	63	81	63	38	56	94	31	31	13	94

3.3 PAN, PPN, and MPAN Relationships

Figure 8 shows the relationship between point measurements of PPN and PAN for the FRAPPÉ campaign. The ratio of PPN/PAN has been used previously to indicate the relative importance of PAN precursor species. PAN can be formed from virtually any VOC, and the immediate precursors are the oxidation intermediates acetaldehyde, acetone, and methylglyoxal [*Fischer et al.*, 2014]. The main intermediate precursor for PPN is propanal [*Roberts et al.*, 2001; *Roberts et al.*, 2007]. The reactions between 1-butene and propane with the OH radical form propanal with 94% and 28% yields, respectively [*Atkinson et al.*, 1985; *Droege and Tully*, 1986]. The low yield of propanal formation via propane may be due to OH preferentially abstracting a hydrogen from the center carbon of propane. However, *Gilman et al.* [2013] found that the mean propane mixing ratio at the BAO tower (27 ppbv) is much greater than that reported in other U.S. cities, such as Houston, TX (6.7 ppbv) [*Gilman et al.*, 2009]. Hence the large propane abundance can potentially be a large propanal source for the NFRMA. Propanal can also be formed through the oxidation of the biogenic molecule cis-3-hexenol by OH [*D Grosjean et al.*, 1993], however, fluxes of cis-3-hexenol are typically small compared to isoprene [*Williams et al.*, 1997]. MPAN is formed during isoprene oxidation via the oxidation intermediate methacrolein [*Bertman and Roberts*, 1991; *Nouaime et al.*, 1998; *Tuazon and Atkinson*, 1990a; *Williams et al.*, 1997], but there is evidence that vehicle exhaust can also be a direct source of both isoprene and methacrolein [*Biesenthal and Shepson*, 1997; *Jonsson et al.*, 1985; *McLaren et al.*, 1996; *Schauer et al.*, 1999; 2002].

Previous studies in the southern U.S. found that PPN/PAN ratios greater than approximately 15% indicate that anthropogenic emissions dominate the photochemistry [*Roberts*

et al., 2003; *Roberts et al.*, 1998; *Williams et al.*, 1997]. The measurements made by *Roberts et al.* [2003] were in a region (Houston, TX) impacted by the oil and gas industry. The mean mixing ratio of light alkanes (*e.g.* ethane and propane) in the Houston region based on measurements made during the summer of 2006 were an order of magnitude less than that found at the BAO tower during winter 2011, although the maximum values were similar [*Gilman et al.*, 2013; *Gilman et al.*, 2009].

The PPN/PAN ratio observed at the BAO tower during FRAPPÉ, determined by RMA, was 21%. The PPN/PAN scatter plot obtained from measurements at the BAO tower also showed very little scatter (R^2 = 92%) compared to that of other ground sites [*Roberts et al.*, 2003; *Roberts et al.*, 1998] in the southern U.S. and lacked a wind or time of day dependence, further providing evidence of a lack of variability in VOC chemistry (see Appendix for wind/time of day dependencies). The MPAN/PAN ratio was <5%, indicating very little influence of isoprene chemistry compared to published datasets in other regions [*Roberts et al.*, 2003; *Roberts et al.*, 2007; *Roberts et al.*, 1998]. The NCAR C-130 data were confined to the same area and height as mentioned above, and the PPN/PAN ratio in this subset of data was also found to be 21% (via RMA). A similar ratio (22%) was also observed in PANs data obtained from the Uintah Basin in Utah, a rural region with substantial oil and gas production [*Patrick Veres*, personal communication].

Ridley et al. [1990] measured PANs species at Niwot Ridge, approximately 30 km west of Boulder at 3050 m ASL from 16 June to 31 July 1987, and at the NCAR Mesa Lab near Boulder from 30 May to 10 June and from 11 August to 24 September 1987. These data indicate

that PPN/PAN ratios in 1987 at these locations were dependent on wind direction and ranged from ~4% when winds were westerly, coming from the remote mountains of Colorado, to ~15% when winds were easterly, indicative of impact from the urban Colorado Front Range. The highest daytime PPN/PAN ratios measured at BAO during FRAPPÉ did not have a clear wind dependence (see Figure 9). The ratios measured were also greater than those measured by *Ridley et al.* [1990].

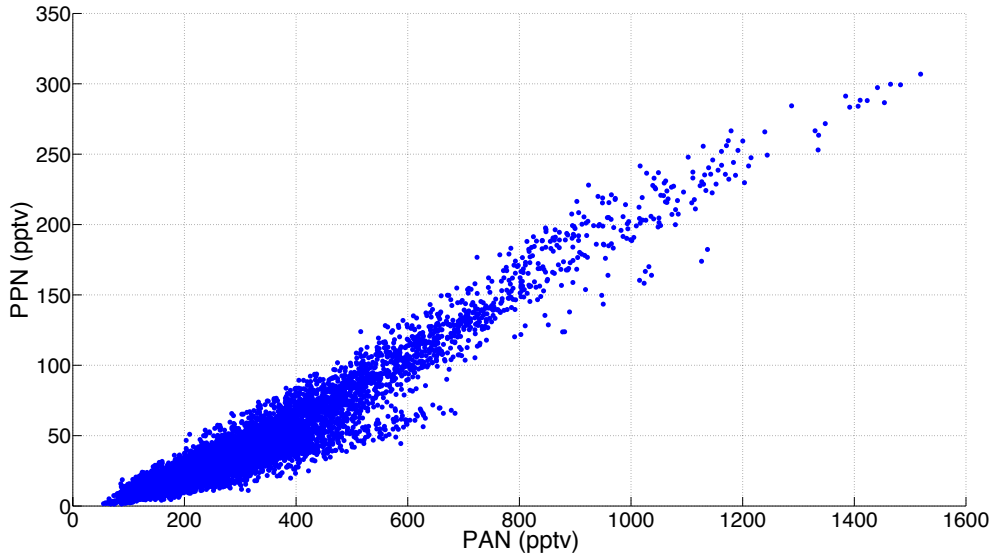

Figure 8: Simultaneous 5-minute point PPN versus PAN observations from BAO for the entire FRAPPÉ campaign.

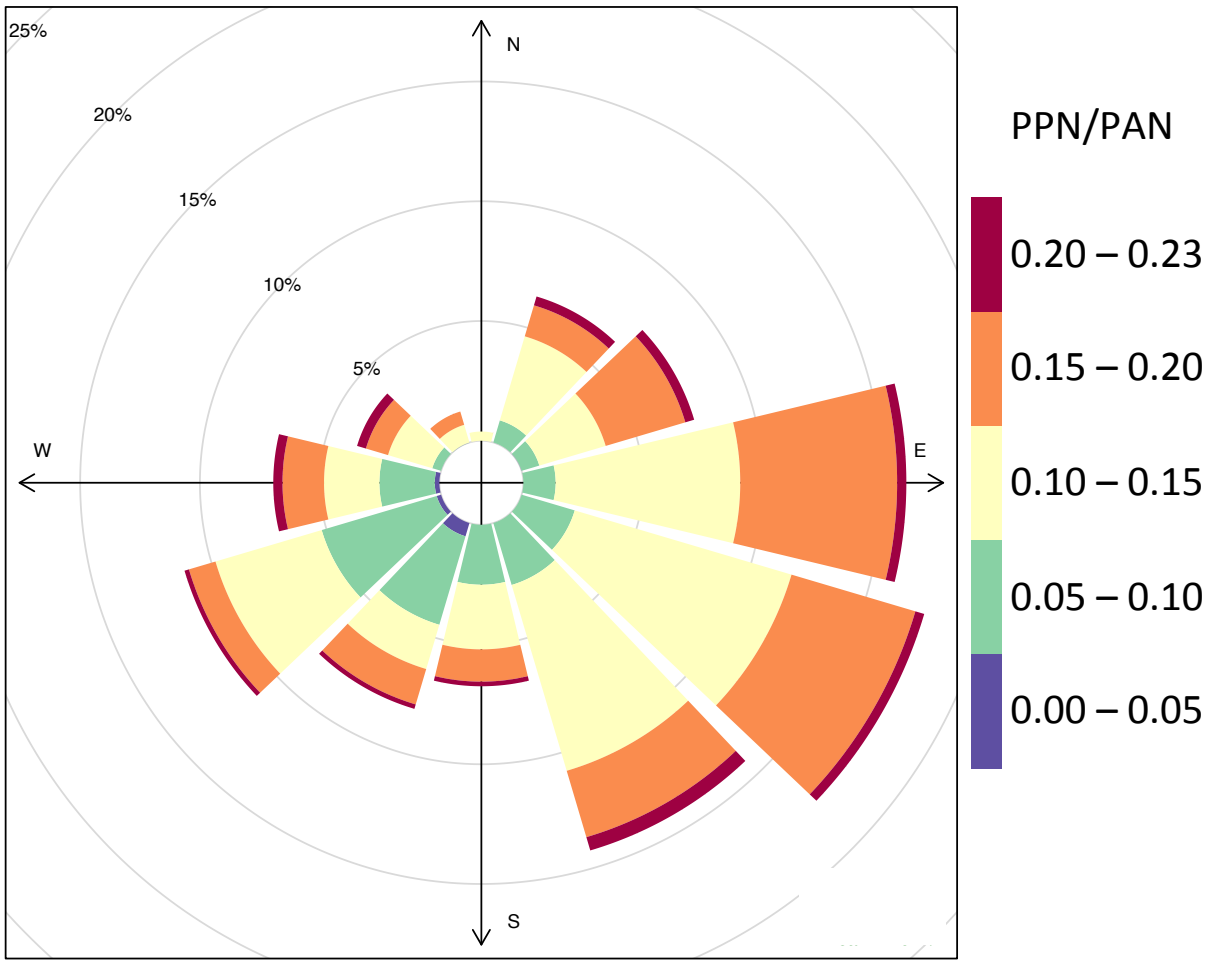

Figure 9: PPN/PAN pollution rose for daytime (6 MDT to 18 MDT) observations. The thickness of the bars represent the frequency that a PPN/PAN ratio was observed at a given wind direction. The wind direction bin angle is 30 degrees.

3.4 Contribution of Biogenic Hydrocarbons to Ozone Production

Williams et al. [1997] used PAN, PPN, and MPAN measured during the 1995 Southern Oxidant Study (SOS) to estimate the contribution of isoprene chemistry to O_3 production with the following assumptions: 1) isoprene and methacrolein sources from vehicle exhaust were minor, 2) the biogenic cis-3-hexenol had a negligible contribution to PPN production, 3) PANs and O_3 were under a dynamic steady state, and 4) the PANs species had similar loss rates. We used a similar approach to estimate the contribution of isoprene chemistry to O_3 abundances at

the BAO tower during FRAPPÉ. A multivariate least-squares analysis (Equation 1) was used to predict PAN abundance from a combination of anthropogenic VOC source (PPN) and a biogenic VOC source (MPAN). As discussed above, the PPN to PAN ratios measured at BAO indicate that anthropogenic VOCs play a dominant role in the photochemistry in this region. The mixture of VOCs measured at BAO during past campaigns indicate that propane and other light alkanes contribute 24 - 55% of the total OH reactivity attributed to VOCs [*Gilman et al.*, 2013; *Swarthout et al.*, 2013].

$$[Estimated\ PAN] = 2.54[MPAN] + 4.23[PPN] + 94.5 \quad (1)$$

Figure 10a presents a scatter plot of the daytime hourly averaged estimated PAN, calculated using Equation 1, versus the daytime hourly averaged measured PAN. There is a strong linear relationship ($R^2 \sim 95\%$) between the predicted and measured value, reflecting the strong and consistent relationship between PPN and PAN at this site (Figure 8). There was also a positive relationship between PAN and O_3 during FRAPPÉ, although the range of PAN and O_3 mixing ratios measured at BAO during FRAPPÉ was smaller than that measured during the 1995 SOS (see Figure 10b). Using Equation 2, where α (2.54) and β (4.23) represent the coefficients resulting from the multivariate least-squares analysis for MPAN and PPN, respectively (see Equation 1), and $[O_{3Bckg}]$ represents the background O_3 mixing ratio, the contribution to total O_3 from isoprene was found to not exceed 20%, regardless of $\left[O_{3Bckg}\right]$ chosen (ranging from 35 ppbv to 65 ppbv, see Appendix), during FRAPPÉ (Figure 11). For Figure 11, the $\left[O_{3Bckg}\right]$ chosen was 45 ppbv, a background mixing ratio most representative of the western U.S. [*Cooper et al.*, 2015]. The highest values of *Isoprene O_3* all consistently occurred on 19 July (red data

points on Figure 11). Regional winds showed a consistent downslope wind until about 10 MDT on this day. Hourly O_3 mixing ratios at BAO exceeded 80 ppbv on 22, 23, 28, and 29 July (Figure 11). Two Front Range O_3 monitoring sites, Rocky Flats North (39.91°N 105.19°W) and NREL (39.74°N 105.18°W), recorded 1st maximum O_3 values of 82 and 79 ppbv, respectively, on 22 July (https://drcog.org/sites/drcog/files/event-materials/2014%20Ozone%20Season%20Update.pdf). Figure 11 suggests that the contribution of isoprene chemistry to hourly average O_3 mixing ratios at BAO was less than 6 ppbv on this day.

$$[Isoprene\ O_3] = \left([O_3] - [O_{3Bckg}]\right) * \frac{\alpha[MPAN]}{(\alpha[MPAN]+\beta[PPN])} \quad (2)$$

MPAN measured during FRAPPÉ had a mean mixing ratio of 9 pptv with a maximum of 36 pptv (see Table 1). These MPAN abundances are small compared to those measured during previous campaigns in the eastern and southern U.S. The maximum mixing ratio observed at BAO is comparable to the mean mixing ratio observed in other locations. For example, mean and maximum values of 27 and 371 pptv were observed during the 2002 New England Air Quality Study [*Roberts et al.*, 2007], mean and maximum values of 15 and 210 pptv were observed during the 2000 Texas Air Quality Study [*Roberts et al.*, 2003], and mean and maximum values of 30 and 150 pptv were observed during the 1995 Southern Oxidant Study [*Nouaime et al.*, 1998].

Here we examine several of the assumptions underpinning the *Williams et al.* [1997] analysis and whether they are appropriate for the Colorado Front Range. Biogenic isoprene

emissions in the Colorado Front Range are expected to be low because broad-leafed vegetation is not abundant in Colorado [*Millet et al.*, 2008]. Vehicle emissions of isoprene and methacrolein may be significant in this region, and thus we hypothesize that a fraction of MPAN formation may be driven by non-biogenic emissions [*Biesenthal and Shepson*, 1997; *Jonsson et al.*, 1985; *McLaren et al.*, 1996; *Schauer et al.*, 1999; 2002]. To explore this, we calculated the ratio of the sum of daytime anthropogenic methacrolein (MACR) and isoprene emissions (Isop1) to the sum of total sources (biogenic direct isoprene emissions and anthropogenic sources). Anthropogenic emissions were obtained from the 2011 NEI and total daytime biogenic direct isoprene (Isop2) emissions were calculated from the MEGAN model. We estimated the fraction of MPAN formation from anthropogenic emissions (Anth. Fraction) (Equation 3). α_1 represents the fraction of isoprene that is oxidized to methacrolein, assumed to be approximately 25% based on isoprene oxidation under high NO_x conditions [*Galloway et al.*, 2011; *Tuazon and Atkinson*, 1990b]. β_1 represents the fraction of methacrolein that is oxidized to MPAN, assumed to be 50% [*Orlando et al.*, 1999; *Tuazon and Atkinson*, 1990a].

$$Anth.Fraction = \frac{\sum(\beta_1 MACR + \beta_1 \alpha_1 Isop1)}{\sum(\beta_1 MACR + \beta_1 \alpha_1 Isop1 + \beta_1 \alpha_1 Isop2)} \quad (3)$$

The calculation was done for every hour between 7 am and 9 pm over the domain of the Colorado Front Range (106 to 104°W and 39.5 to 40.6°N). We found that the biogenic emissions of isoprene were several orders of magnitude larger than the anthropogenic emissions of both methacrolein and isoprene (Table 3). The same was true for the smaller domain of 105.29 to 104°W and 39.5 to 40.6°N (Table 3), encompassing the cities between Denver and Fort Collins and between Boulder and Greeley, but not the mountains to the west. In studies in the southern

U.S. where biogenic isoprene emissions are large, the biogenic contribution to PPN has been neglected [*Roberts et al.*, 1998], with a supporting piece of evidence being the low PPN/PAN ratios measured over forested regions [*Williams et al.*, 1997]. In the NFRMA, where emissions of isoprene are lower than in the southern U.S. [*Millet et al.*, 2008], it is also expected that there is a negligible biogenic source of PPN. *Williams et al.* [1997] assumed dynamic steady state of the PANs species and O_3. This is a reasonable assumption because we expect warm summer temperatures and high radiation of the Colorado Front Range to create a short thermal lifetime for PAN and a large daytime radical source. Finally, *Williams et al.* [1997] asserted that the PANs considered all have similar loss rates. *Roberts and Bertman* [1992] and *Kirchner et al.* [1999] support this claim.

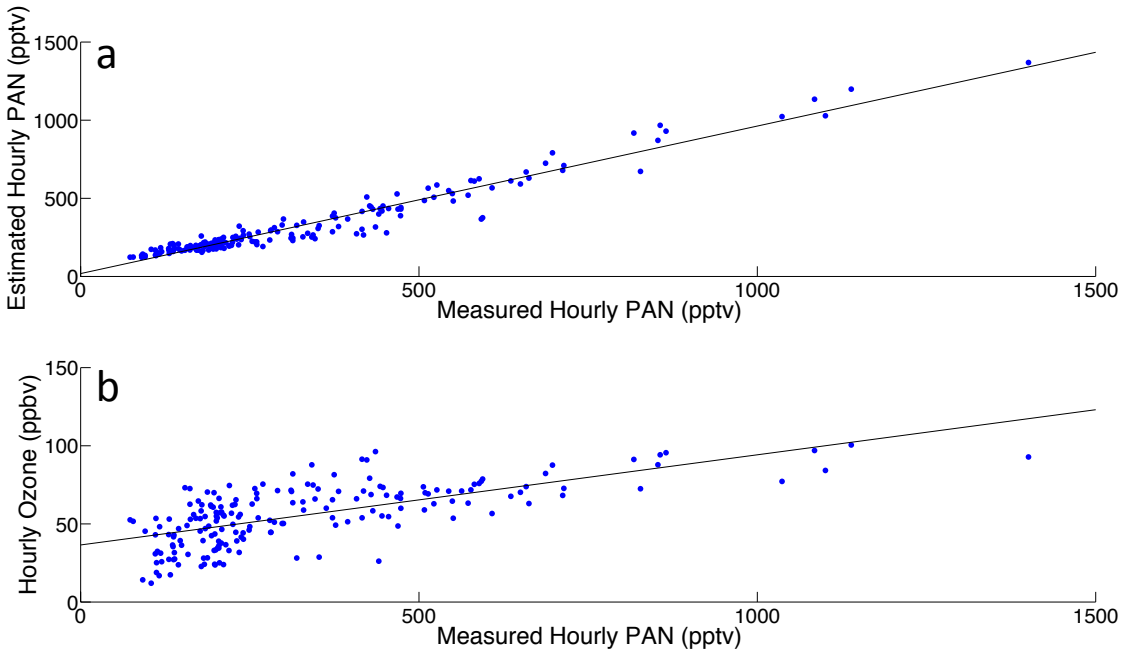

Figure 10: a) Estimated hourly average PAN from MPAN and PPN calculated using Equation 1 versus hourly average measured PAN b) hourly average measured O_3 versus hourly average measured PAN.

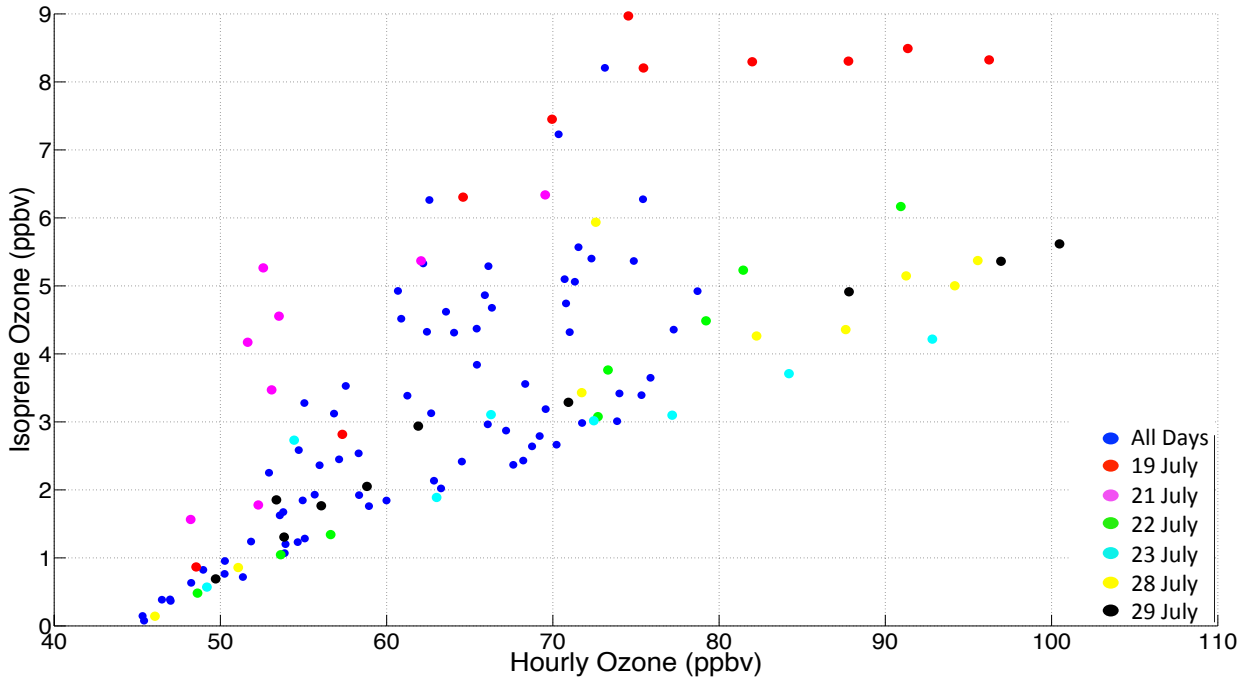

Figure 11: Estimated O_3 from biogenic VOCs (Isoprene Ozone) calculated using Equation 2 versus hourly average measured O_3. $[O_{3Bckg}]$ is set to 45 ppbv for this calculation. The colored values represent specific days.

Table 3: The calculated Anthropogenic Fraction of MPAN for times when traffic is expected to be most active. Anth. Fraction 1 is between 106 and 104°W and Anth. Fraction 2 is between 105.29 and 104°W.

Time (MDT)	Anth. Fraction 1($x10^{-6}$)	Anth. Fraction 2($x10^{-6}$)
7	12.9	42.4
8	6.03	19.8
9	4.67	14.9
10	3.69	11.3
11	3.66	10.1
12	2.92	6.85
13	2.97	6.73
14	3.58	8.70
15	5.09	14.9
16	6.98	23.0
17	8.88	31.7
18	13.1	42.0
19	47.2	152
20	543	2090
21	520000	976000

Chapter 4: Summary and Suggestions for Future Work

We present measurements of PAN, PPN, and MPAN from the BAO Tower during the summer 2014 FRAPPÉ field intensive. The measurements were made with the custom-built NCAR PAN GC-ECD [*Flocke et al.*, 2005]. A visual classification of FLEXPART back trajectories generated throughout FRAPPÉ for BAO showed that 1) elevated PAN is associated with recirculation in the region, but 2) recirculation was a common occurrence during the FRAPPÉ period and not exclusive to periods with active photochemistry. Observations of PPN/PAN ratios made during summer 2014 at BAO do not show a clear and consistent wind sector dependence.

The PPN/PAN ratio observed at BAO during the summer of 2014 was 21%, and this reflects the dominant role that anthropogenic VOCs play in the regional photochemistry. The observed ratio also showed little scatter (R^2 = 92%), suggesting that there was relatively little variability in the VOC chemistry compared to other regions [*Roberts et al.*, 2003; *Roberts et al.*, 1998] where the scatter of PPN/PAN data was much greater.

We used the relative abundance of MPAN and PPN to estimate the contribution of biogenic VOCs to O_3 production. This analysis shows that during the summer of 2014, the maximum contribution to O_3 mixing ratios from isoprene oxidation was consistently less than 20%. This was determined by assuming, among other things, that all MPAN measured was formed via biogenic isoprene oxidation and all PPN measured was formed via anthropogenic hydrocarbon oxidation. These assumptions appear to be reasonable for the NFRMA, despite the

minimal broad-leaf vegetation. The findings of this study suggest that anthropogenic emissions are the largest drivers of photochemistry in the NFRMA.

Consistent with the past observations of VOCs at BAO [*Gilman et al.*, 2013; *Pétron et al.*, 2012; *Swarthout et al.*, 2013], the high and persistent observed PPN/PAN ratio at BAO indicates that anthropogenic VOCs dominate the VOC-NO_x photochemistry in the NFRMA. A high and relatively consistent ratio was also observed in the Uintah Basin during winter 2013 [*Patrick Veres*, personal communication]. We hypothesize that this ratio may represent light alkane chemistry. To fully understand the utility of PANs as tracers of specific chemistry, it is important to identify the specific emissions and immediate precursors responsible for the observed ratios. The Dynamically Simple Model of Atmospheric Chemical Complexity (DSMACC) [*Edwards et al.*, 2011; *Emmerson and Evans*, 2009; *Stone et al.*, 2010] can be a tool for doing this. DSMACC is a zero-dimensional box model that uses chemistry schemes generated with the Master Chemical Mechanism Version 3.3.1 (http://mcm.leeds.ac.uk/MCM) and the Kinetic Preprocessor (KPP) for integration [*Sandu and Sander*, 2006]. It has been successfully used to simulate abundances of O_3, PPN, PAN, and other key photochemical species in other oil and gas basins in the U.S. [*Edwards et al.*, 2013; *Edwards et al.*, 2014]. It could be used to determine which hydrocarbons and oxidation pathways contributed to the PPN/PAN ratio observed in summer 2014.

Measurements of trace gases and aerosols were made from aircraft in several different western U.S. tight oil and shale gas basins, including the DJB, as part of the NOAA Shale Oil and Natural Gas NEXus (SONGNEX) campaign in the spring of 2015 (March through May).

Measurements of the PANs, CO, CO_2, CH_4, H_2O, O_3, NO_y, and light alkanes were made at the BAO Tower during the SONGNEX period and again in summer 2015 between July and September. The next step in the analysis of the FRAPPÉ PANs data is to compare it to these more recent observations. Summer 2014 was considered a relatively "clean" year, with only one NFRMA O_3 monitor (NREL) exceeding the then 4th Maximum 8-hour Average Value of 75 ppbv in the NFRMA. There were also no major impacts of biomass burning smoke, which can have significant impacts in the region, during summer 2014, either fresh or aged. The maximum hourly average O_3 observed at BAO was 100 ppbv and hourly average O_3 values exceeded 75 ppbv on 16 days during the summer of 2014. A preliminary analysis of O_3 measurements from summer 2015 indicates higher O_3 at BAO with 21 days exceeding point values of 75 ppbv between 28 June and 7 September. The region was also influenced by smoke plumes transported from fires in the Pacific Northwest during two multi-day periods. The availability of VOC data at the same site for 2015 will also help constrain any photochemical box modeling.

References

Atkinson, R., E. C. Tuazon, and W. P. L. Carter (1985), Extent of H-atom abstraction from the reaction of the OH radical with 1-butene under atmospheric conditions, *International Journal of Chemical Kinetics*, *17*(7), 725-734.

Ayers, G. P. (2001), Comment on regression analysis of air quality data, *Atmospheric Environment*, *35*(13), 2423-2425.

Bertman, S. B., and J. M. Roberts (1991), A PAN analog from isoprene photooxidation, *Geophysical Research Letters*, *18*(8), 1461-1464.

Biesenthal, T. A., and P. B. Shepson (1997), Observations of anthropogenic inputs of the isoprene oxidation products methyl vinyl ketone and methacrolein to the atmosphere, *Geophysical Research Letters*, *24*(11), 1375-1378.

Brioude, J., et al. (2013), The Lagrangian particle dispersion model FLEXPART-WRF version 3.1, *Geosci. Model Dev.*, *6*(6), 1889-1904.

Brodin, M., D. Helmig, and S. Oltmans (2010), Seasonal ozone behavior along an elevation gradient in the Colorado Front Range Mountains, *Atmospheric Environment*, *44*(39), 5305-5315.

Brown, S. S., H. Stark, and A. R. Ravishankara (2002), Cavity ring-down spectroscopy for atmospheric trace gas detection: application to the nitrate radical (NO3), *Appl. Phys. B*, *75*(2-3), 173-182.

Brown, S. S., et al. (2013), Nitrogen, Aerosol Composition, and Halogens on a Tall Tower (NACHTT): Overview of a wintertime air chemistry field study in the front range urban corridor of Colorado, *Journal of Geophysical Research: Atmospheres*, *118*(14), 8067-8085.

Callahan, S., E. Fischer, Y. Zhou, and B. C. Sive (2014), PAN Among the Peaks: A preliminary analysis of new peroxyacetyl nitrate (PAN) measurements in Rocky Mountain National Park, in *2014 AGU Fall Meeting*, edited, San Francisco.

Cooper, O. R., A. O. Langford, D. D. Parrish, and D. W. Fahey (2015), Challenges of a lowered U.S. ozone standard, *Science*, *348*(6239), 1096-1097.

Cooper, O. R., R.-S. Gao, D. Tarasick, T. Leblanc, and C. Sweeney (2012), Long-term ozone trends at rural ozone monitoring sites across the United States, 1990–2010, *Journal of Geophysical Research: Atmospheres*, *117*(D22), D22307.

Cooper, O. R., et al. (2010), Increasing springtime ozone mixing ratios in the free troposphere over western North America, *Nature*, *463*(7279), 344-348.

Crook, N. A., T. L. Clark, and M. W. Moncrieff (1990), The Denver Cyclone. Part I: Generation in Low Froude Number Flow, *Journal of the Atmospheric Sciences*, *47*(23), 2725-2742.

Droege, A. T., and F. P. Tully (1986), Hydrogen-atom abstraction from alkanes by hydroxyl. 3. Propane, *The Journal of Physical Chemistry*, *90*(9), 1949-1954.

Dubé, W. P., S. S. Brown, H. D. Osthoff, M. R. Nunley, S. J. Ciciora, M. W. Paris, R. J. McLaughlin, and A. R. Ravishankara (2006), Aircraft instrument for simultaneous, in situ measurement of NO3 and N2O5 via pulsed cavity ring-down spectroscopy, *Review of Scientific Instruments*, *77*(3), 034101.

Edwards, P. M., et al. (2011), Hydrogen oxide photochemistry in the northern Canadian spring time boundary layer, *Journal of Geophysical Research: Atmospheres*, *116*(D22), D22306.

Edwards, P. M., et al. (2013), Ozone photochemistry in an oil and natural gas extraction region during winter: simulations of a snow-free season in the Uintah Basin, Utah, *Atmos. Chem. Phys.*, *13*(17), 8955-8971.

Edwards, P. M., et al. (2014), High winter ozone pollution from carbonyl photolysis in an oil and gas basin, *Nature*, *514*(7522), 351-354.

Emmerson, K. M., and M. J. Evans (2009), Comparison of tropospheric gas-phase chemistry schemes for use within global models, *Atmos. Chem. Phys.*, *9*(5), 1831-1845.

Fischer, E. V., A. Pszenny, W. Keene, J. Maben, A. Smith, A. Stohl, and R. Talbot (2006), Nitric acid phase partitioning and cycling in the New England coastal atmosphere, *Journal of Geophysical Research: Atmospheres*, *111*(D23), D23S09.

Fischer, E. V., et al. (2014), Atmospheric peroxyacetyl nitrate (PAN): a global budget and source attribution, *Atmos. Chem. Phys.*, *14*(5), 2679-2698.

Flocke, F., A. Weinheimer, A. Swanson, J. Roberts, R. Schmitt, and S. Shertz (2005), On the Measurement of PANs by Gas Chromatography and Electron Capture Detection, *J Atmos Chem*, *52*(1), 19-43.

Fuchs, H., W. P. Dubé, S. J. Ciciora, and S. S. Brown (2008), Determination of Inlet Transmission and Conversion Efficiencies for in Situ Measurements of the Nocturnal Nitrogen Oxides, NO3, N2O5 and NO2, via Pulsed Cavity Ring-Down Spectroscopy, *Analytical Chemistry*, *80*(15), 6010-6017.

Fuchs, H., W. P. Dubé, B. M. Lerner, N. L. Wagner, E. J. Williams, and S. S. Brown (2009), A Sensitive and Versatile Detector for Atmospheric NO2 and NOX Based on Blue Diode Laser Cavity Ring-Down Spectroscopy, *Environmental Science & Technology*, *43*(20), 7831-7836.

Galloway, M. M., A. J. Huisman, L. D. Yee, A. W. H. Chan, C. L. Loza, J. H. Seinfeld, and F. N. Keutsch (2011), Yields of oxidized volatile organic compounds during the OH radical initiated oxidation of isoprene, methyl vinyl ketone, and methacrolein under high-NOx conditions, *Atmos. Chem. Phys.*, *11*(21), 10779-10790.

Gilman, J. B., B. M. Lerner, W. C. Kuster, and J. A. de Gouw (2013), Source Signature of Volatile Organic Compounds from Oil and Natural Gas Operations in Northeastern Colorado, *Environmental Science & Technology*, *47*(3), 1297-1305.

Gilman, J. B., et al. (2009), Measurements of volatile organic compounds during the 2006 TexAQS/GoMACCS campaign: Industrial influences, regional characteristics, and diurnal dependencies of the OH reactivity, *Journal of Geophysical Research: Atmospheres*, *114*(D7), D00F06.

Grosjean, D., E. L. Williams, and E. Grosjean (1993), A biogenic precursor of peroxypropionyl nitrate: atmospheric oxidation of cis-3-hexen-1-ol, *Environmental Science & Technology*, *27*(5), 979-981.

Grosjean, E., D. Grosjean, and L. F. Woodhouse (2001), Peroxyacetyl Nitrate and Peroxypropionyl Nitrate during SCOS 97-NARSTO, *Environmental Science & Technology*, *35*(20), 4007-4014.

Guenther, A., T. Karl, P. Harley, C. Wiedinmyer, P. I. Palmer, and C. Geron (2006), Estimates of global terrestrial isoprene emissions using MEGAN (Model of Emissions of Gases and Aerosols from Nature), *Atmos. Chem. Phys.*, *6*(11), 3181-3210.

Hahn, C. (1981), A study of the diurnal behavior of boundary-layer winds at the Boulder Atmospheric Observatory, *Boundary-Layer Meteorol*, *21*(2), 231-245.

Jerrett, M., R. T. Burnett, C. A. Pope, K. Ito, G. Thurston, D. Krewski, Y. Shi, E. Calle, and M. Thun (2009), Long-Term Ozone Exposure and Mortality, *New England Journal of Medicine*, *360*(11), 1085-1095.

Jonsson, A., K. A. Persson, and V. Grigoriadis (1985), Genotoxic Air Pollutants Measurements of some low molecular-weight oxygenated, aromatic, and chlorinated hydrocarbons in ambient air and in vehicle emissions, *Environment International*, *11*(2), 383-392.

Kaimal, J. C., and J. E. Gaynor (1983), The Boulder Atmospheric Observatory, *Journal of Climate and Applied Meteorology*, *22*(5), 863-880.

Kirchner, F., A. Mayer–Figge, F. Zabel, and K. H. Becker (1999), Thermal stability of Peroxynitrates, *International Journal of Chemical Kinetics*, *31*(2), 127-144.

McLaren, R., D. L. Singleton, J. Y. K. Lai, B. Khouw, E. Singer, Z. Wu, and H. Niki (1996), Analysis of motor vehicle sources and their contribution to ambient hydrocarbon distributions at urban sites in Toronto during the Southern Ontario oxidants study, *Atmospheric Environment*, *30*(12), 2219-2232.

Millet, D. B., D. J. Jacob, K. F. Boersma, T.-M. Fu, T. P. Kurosu, K. Chance, C. L. Heald, and A. Guenther (2008), Spatial distribution of isoprene emissions from North America derived from formaldehyde column measurements by the OMI satellite sensor, *Journal of Geophysical Research: Atmospheres*, *113*(D2), D02307.

Nouaime, G., S. B. Bertman, C. Seaver, D. Elyea, H. Huang, P. B. Shepson, T. K. Starn, D. D. Riemer, R. G. Zika, and K. Olszyna (1998), Sequential oxidation products from tropospheric isoprene chemistry: MACR and MPAN at a NO x -rich forest environment in the southeastern United States, *Journal of Geophysical Research: Atmospheres*, *103*(D17), 22463-22471.

Orlando, J. J., G. S. Tyndall, and S. E. Paulson (1999), Mechanism of the OH-initiated oxidation of methacrolein, *Geophysical Research Letters*, *26*(14), 2191-2194.

Parrish, D. D., D. B. Millet, and A. H. Goldstein (2009), Increasing ozone in marine boundary layer inflow at the west coasts of North America and Europe, *Atmos. Chem. Phys.*, *9*(4), 1303-1323.

Pétron, G., et al. (2014), A new look at methane and nonmethane hydrocarbon emissions from oil and natural gas operations in the Colorado Denver-Julesburg Basin, *Journal of Geophysical Research: Atmospheres*, *119*(11), 2013JD021272.

Pétron, G., et al. (2012), Hydrocarbon emissions characterization in the Colorado Front Range: A pilot study, *Journal of Geophysical Research: Atmospheres*, *117*(D4), D04304.

Ridley, B. A., et al. (1990), The behavior of some organic nitrates at Boulder and Niwot Ridge, Colorado, *Journal of Geophysical Research: Atmospheres*, *95*(D9), 13949-13961.

Roberts, J. M., and S. B. Bertman (1992), The thermal decomposition of peroxyacetic nitric anhydride (PAN) and peroxymethacrylic nitric anhydride (MPAN), *International Journal of Chemical Kinetics*, *24*(3), 297-307.

Roberts, J. M., C. A. Stroud, B. T. Jobson, M. Trainer, D. Hereid, E. Williams, F. Fehsenfeld, W. Brune, M. Martinez, and H. Harder (2001), Application of a sequential reaction model to PANs and aldehyde measurements in two urban areas, *Geophysical Research Letters*, *28*(24), 4583-4586.

Roberts, J. M., et al. (2003), An examination of the chemistry of peroxycarboxylic nitric anhydrides and related volatile organic compounds during Texas Air Quality Study 2000 using ground-based measurements, *Journal of Geophysical Research: Atmospheres*, *108*(D16), 4495.

Roberts, J. M., et al. (2007), Measurements of PANs during the New England Air Quality Study 2002, *Journal of Geophysical Research: Atmospheres*, *112*(D20), D20306.

Roberts, J. M., et al. (2004), Measurement of peroxycarboxylic nitric anhydrides (PANs) during the ITCT 2K2 aircraft intensive experiment, *Journal of Geophysical Research: Atmospheres*, *109*(D23), D23S21.

Roberts, J. M., et al. (1998), Measurements of PAN, PPN, and MPAN made during the 1994 and 1995 Nashville Intensives of the Southern Oxidant Study: Implications for regional ozone production from biogenic hydrocarbons, *Journal of Geophysical Research: Atmospheres*, *103*(D17), 22473-22490.

Russell, A. R., L. C. Valin, and R. C. Cohen (2012), Trends in OMI NO2 observations over the United States: effects of emission control technology and the economic recession, *Atmos. Chem. Phys.*, *12*(24), 12197-12209.

Sandu, A., and R. Sander (2006), Technical note: Simulating chemical systems in Fortran90 and Matlab with the Kinetic PreProcessor KPP-2.1, *Atmos. Chem. Phys.*, *6*(1), 187-195.

Schauer, J. J., M. J. Kleeman, G. R. Cass, and B. R. T. Simoneit (1999), Measurement of Emissions from Air Pollution Sources. 2. C1 through C30 Organic Compounds from Medium Duty Diesel Trucks, *Environmental Science & Technology*, *33*(10), 1578-1587.

Schauer, J. J., M. J. Kleeman, G. R. Cass, and B. R. T. Simoneit (2002), Measurement of Emissions from Air Pollution Sources. 5. C1−C32 Organic Compounds from Gasoline-Powered Motor Vehicles, *Environmental Science & Technology*, *36*(6), 1169-1180.

Singh, H. B. (1987), Reactive nitrogen in the troposphere, *Environmental Science & Technology*, *21*(4), 320-327.

Singh, H. B., and P. L. Hanst (1981), Peroxyacetyl nitrate (PAN) in the unpolluted atmosphere: An important reservoir for nitrogen oxides, *Geophysical Research Letters*, *8*(8), 941-944.

Singh, H. B., et al. (1994), Summertime distribution of PAN and other reactive nitrogen species in the northern high-latitude atmosphere of eastern Canada, *Journal of Geophysical Research: Atmospheres*, *99*(D1), 1821-1835.

Singh, H. B., et al. (1985), Relationship between peroxyacetyl nitrate and nitrogen oxides in the clean troposphere, *Nature*, *318*(6044), 347-349.

Stohl, A., C. Forster, A. Frank, P. Seibert, and G. Wotawa (2005), Technical note: The Lagrangian particle dispersion model FLEXPART version 6.2, *Atmos. Chem. Phys.*, *5*(9), 2461-2474.

Stone, D., et al. (2010), HOx observations over West Africa during AMMA: impact of isoprene and NOx, *Atmos. Chem. Phys.*, *10*(19), 9415-9429.

Swarthout, R. F., R. S. Russo, Y. Zhou, A. H. Hart, and B. C. Sive (2013), Volatile organic compound distributions during the NACHTT campaign at the Boulder Atmospheric Observatory: Influence of urban and natural gas sources, *Journal of Geophysical Research: Atmospheres*, *118*(18), 10,614-610,637.

Szoke, E. J. (1991), Eye of the Denver Cyclone, *Monthly Weather Review*, *119*(5), 1283-1292.

Thompson, C., J. Hueber, and D. Helmig (2014), Influence of oil and gas emissions on ambient atmospheric non-methane hydrocarbons in residential areas of Northeastern Colorado, *Elementa Science of the Anthropocene*, *2*.

Thurston, G. D., M. Lippmann, M. B. Scott, and J. M. Fine (1997), Summertime haze air pollution and children with asthma, *American Journal of Respiratory and Critical Care Medicine*, *155*(2), 654-660.

Tuazon, E. C., and R. Atkinson (1990a), A product study of the gas-phase reaction of Methacrolein with the OH radical in the presence of NOx, *International Journal of Chemical Kinetics*, *22*(6), 591-602.

Tuazon, E. C., and R. Atkinson (1990b), A product study of the gas-phase reaction of Isoprene with the OH radical in the presence of NOx, *International Journal of Chemical Kinetics*, *22*(12), 1221-1236.

Volz-Thomas, A., Xueref, I., Schmitt, R. (2002), Automatic gas chromatograph and calibration system for ambient measurements of PAN and PPN, *Environmental science and pollution research*, *9*(Special Issue 4), 72-76.

Warneck, P., and T. Zerbach (1992), Synthesis of peroxyacetyl nitrate in air by acetone photolysis, *Environmental Science & Technology*, *26*(1), 74-79.

Washenfelder, R. A., N. L. Wagner, W. P. Dube, and S. S. Brown (2011), Measurement of Atmospheric Ozone by Cavity Ring-down Spectroscopy, *Environmental Science & Technology*, *45*(7), 2938-2944.

Westerling, A. L., H. G. Hidalgo, D. R. Cayan, and T. W. Swetnam (2006), Warming and Earlier Spring Increase Western U.S. Forest Wildfire Activity, *Science*, *313*(5789), 940-943.

Wiedinmyer, C., S. K. Akagi, R. J. Yokelson, L. K. Emmons, J. A. Al-Saadi, J. J. Orlando, and A. J. Soja (2011), The Fire INventory from NCAR (FINN): a high resolution global model to estimate the emissions from open burning, *Geosci. Model Dev.*, *4*(3), 625-641.

Wilczak, J. M., and J. W. Glendening (1988), Observations and Mixed-Layer Modeling of a Terrain-Induced Mesoscale Gyre: The Denver Cyclone, *Monthly Weather Review*, *116*(12), 2688-2711.

Wilczak, J. M., and T. W. Christian (1990), Case Study of an Orographically Induced Mesoscale Vortex (Denver Cyclone), *Monthly Weather Review*, *118*(5), 1082-1102.

Wild, R. J., et al. (2014), A Measurement of Total Reactive Nitrogen, NOy, together with NO2, NO, and O3 via Cavity Ring-down Spectroscopy, *Environmental Science & Technology*, *48*(16), 9609-9615.

Williams, J., et al. (1997), Regional ozone from biogenic hydrocarbons deduced from airborne measurements of PAN, PPN, and MPAN, *Geophysical Research Letters*, *24*(9), 1099-1102.

Zheng, W., F. M. Flocke, G. S. Tyndall, A. Swanson, J. J. Orlando, J. M. Roberts, L. G. Huey, and D. J. Tanner (2011), Characterization of a thermal decomposition chemical ionization mass spectrometer for the measurement of peroxy acyl nitrates (PANs) in the atmosphere, *Atmos. Chem. Phys.*, *11*(13), 6529-6547.

Appendix

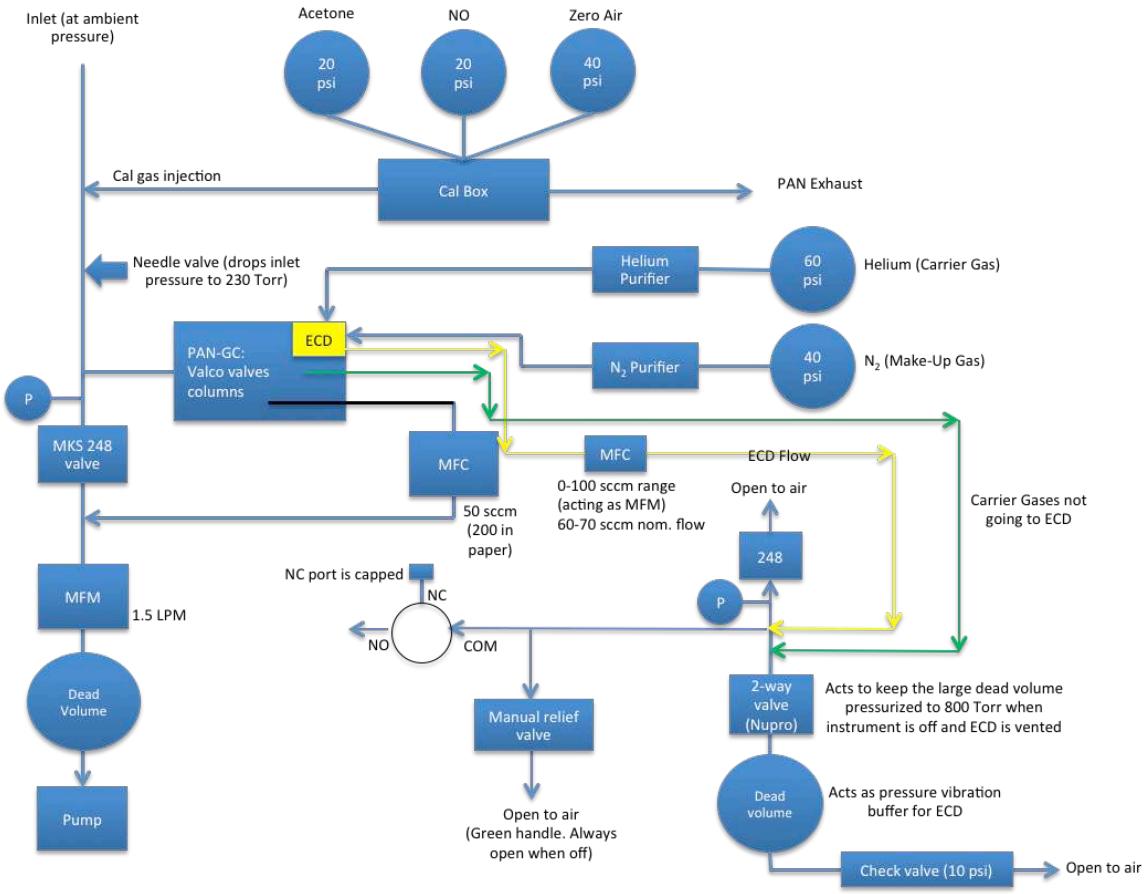

Figure A1: Plumbing diagram for NCAR PAN GC. Arrows represent the direction of gas flow. The yellow arrows represent the ECD exhaust flow (N_2 + He) and the green arrows represent carrier gas (He) not flowing through the ECD. Mass flow controllers, valves, purifiers, the PAN GC and the calibration box are all represented by rectangles. Dead volumes, gas cylinders, and pressure transducers are all represented by circles.

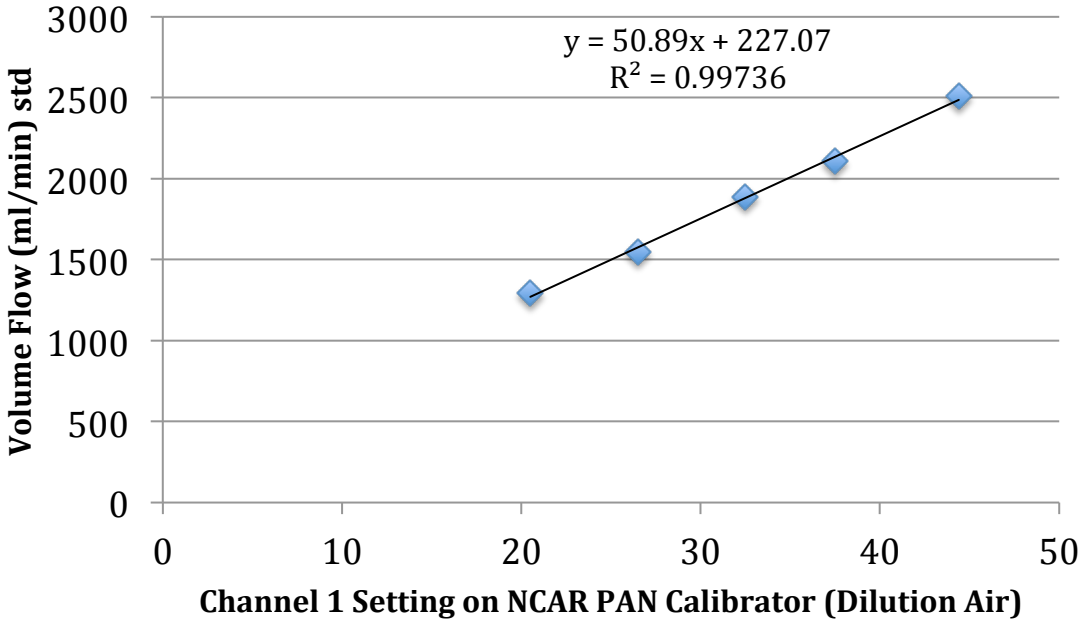
y = 50.89x + 227.07
R² = 0.99736
Volume Flow (ml/min) std
3000
2500
2000
1500
1000
500
0
0
10
20
30
40
50
Channel 1 Setting on NCAR PAN Calibrator (Dilution Air)

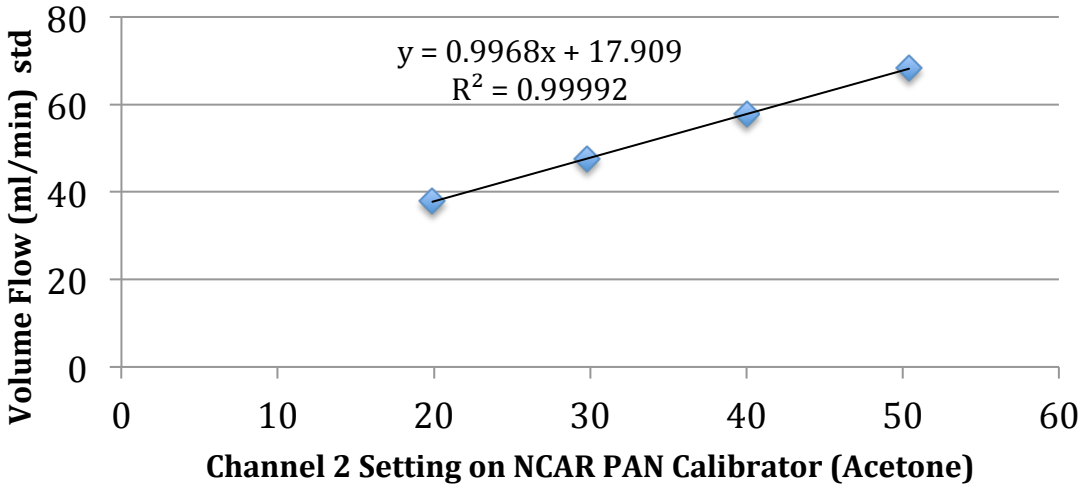
y = 0.9968x + 17.909
R² = 0.99992
Volume Flow (ml/min) std
80
60
40
20
0
0
10
20
30
40
50
60
Channel 2 Setting on NCAR PAN Calibrator (Acetone)

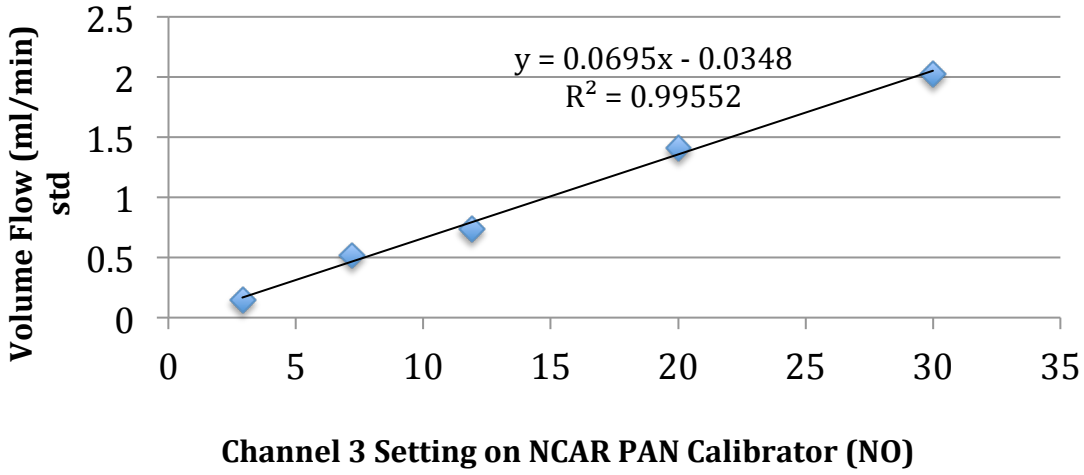

Figure A2: Calibration results for the mass flow controllers (MFC) in the PAN GC calibrator. These tests were performed on 2/18/14 (pre-FRAPPÉ). The precision of each setting, 6, 1 and 3% respectively, was determined by taking the ratio of the standard deviation over the mean of repeated measurements and multiplying by 100%. The standard volume flow for the NO and acetone MFCs was determined by taking the average volume flow of five flow measurements (w/Agilent Flow meter) and multiplying by the ratio of observed pressure over standard pressure and standard temperature over observed temperature. The acetone MFC flow was determined first (with NO flow at zero), then the NO MFC flow was determined as the total flow (NO+acetone) minus a constant acetone flow. The standard flow for the zero air MFC was measured with the MesaLabs Definer. The least squares regressions were determined using Excel.

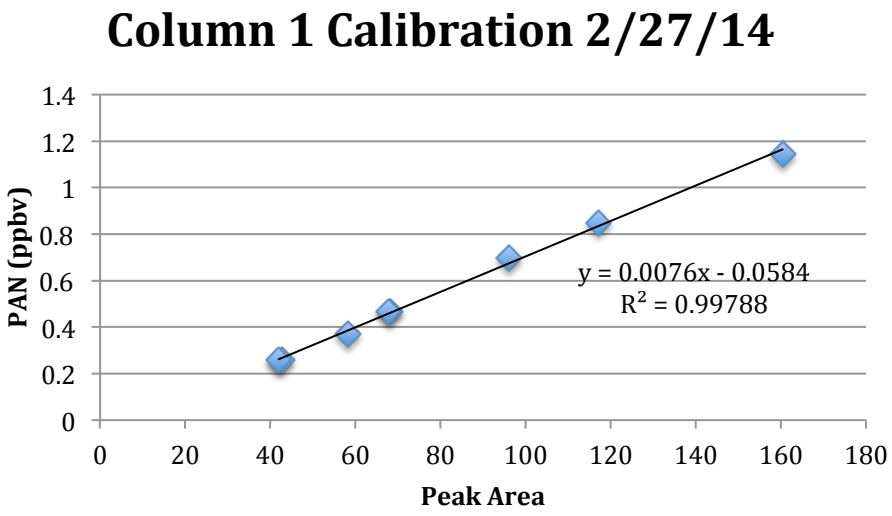

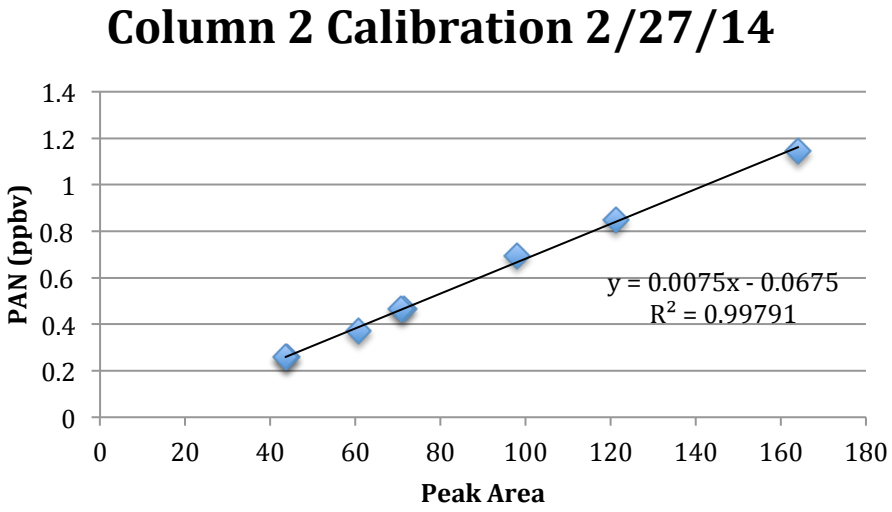

Figure A3: In-lab multi-point calibration on 2/27/14 for both columns. Equation A1 was used to determine the PAN abundance in ppbv, where the 0.969 is the NO calibration value in ppmv, the 0.93 is the calibrator efficiency of PAN formation via acetone photolysis [*Volz-Thomas*, 2002], and the 1000 is the conversion factor between ppmv and ppbv. The peak areas were obtained via integration with Igor (see below). Least squares regressions were obtained with Excel.

$$[PAN\ (ppbv)] = 0.969 * \frac{NO\ Vol.Flow}{Total\ Vol.Flow} * 0.93 * 1000 \qquad \text{Eq. A1}$$

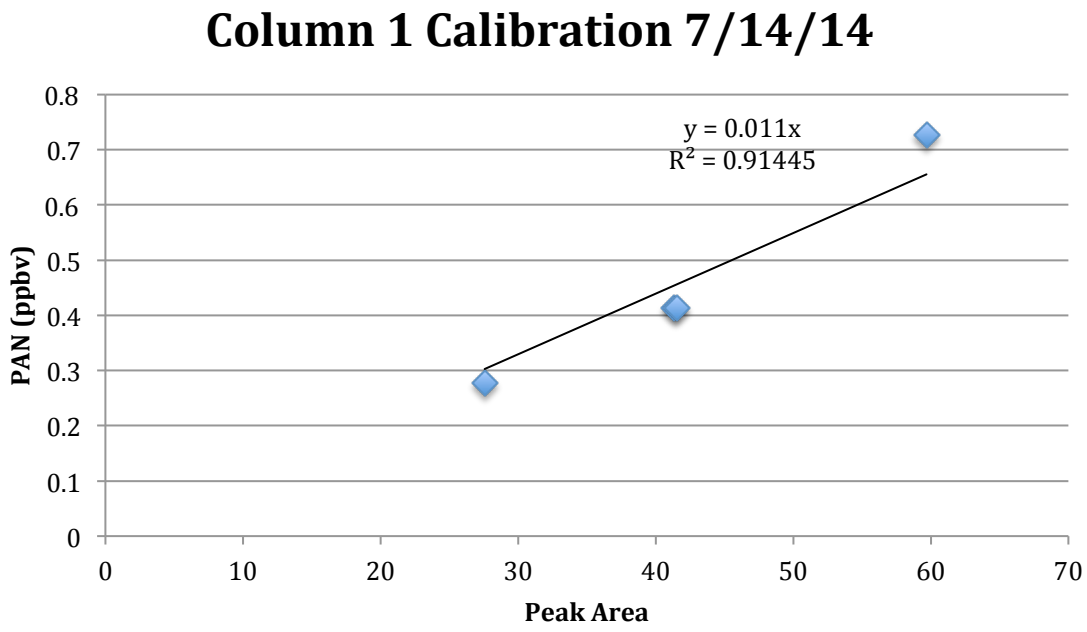

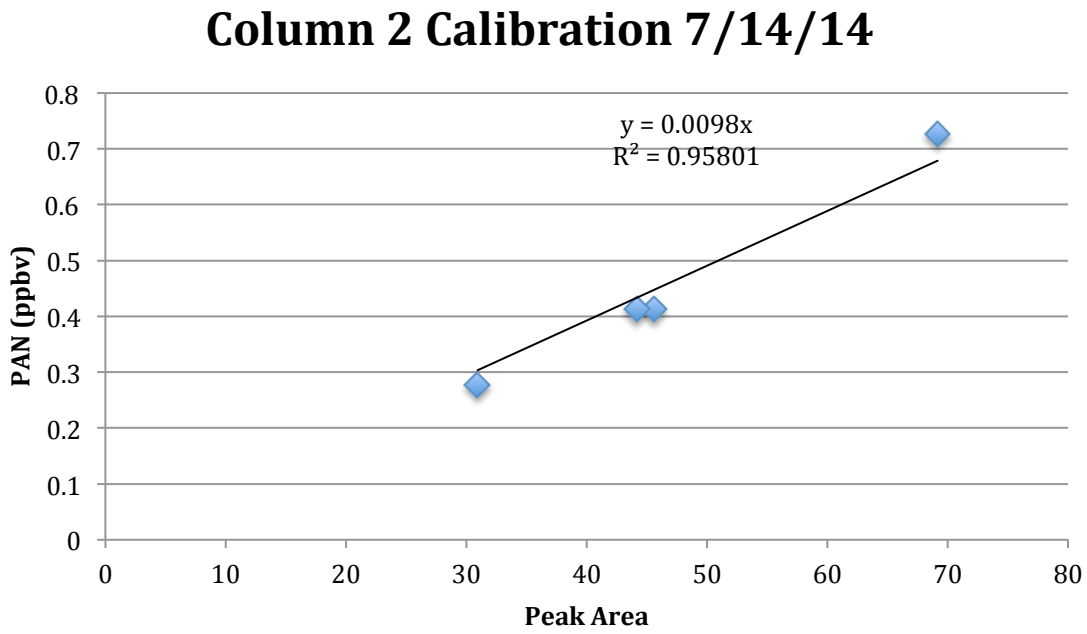

Figure A4: In-field multi-point calibration on 7/14/14 for both columns. Equation A1 was used to determine the PAN abundance. Peak areas were obtained with Igor and the least squares regressions with Excel.

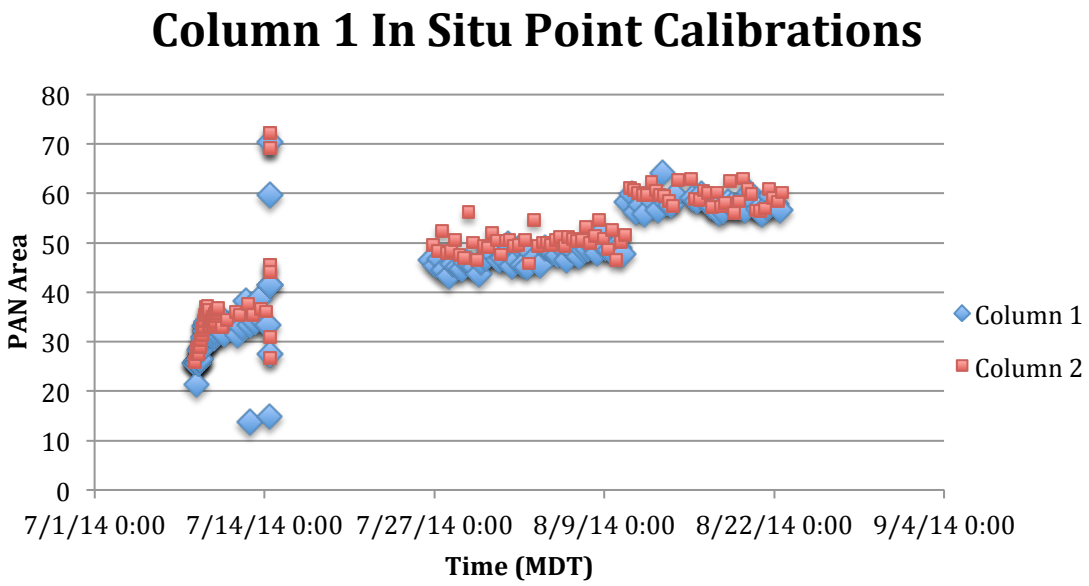

Figure A5: Point calibrations made throughout FRAPPÉ. 7/9 and 7/10 had hourly calibrations while the rest of the campaign had calibrations every 4 hours. A multi-point calibration is also shown on 7/14. The gap between 7/14 and 7/26 was due to the calibrator being accidentally left off. The step on 8/10 represents an increase in the inlet pressure in an attempt to deal with the noisy baselines.

PAN GC uncertainty:
The uncertainty of the calibrator was calculated with Equation A2. The zero air generator was an Environics Series 7000 Zero Air Generator, which is expected to output less than 0.5 ppbv of NO (http://www.environics.com/Product/zero-air-generators/series-7000). The amount of NO in the calibration cylinder was 969 ppbv, therefore, the *Zero Air Uncertainty* is expected to be 0. $Cal.Eff$ is 0.03, corresponding to the calibrator efficiency [*Volz-Thomas*, 2002]. $Calibrator\ Unc.$ was determined to be 0.09.

$$Calibrator\ Unc. = \sqrt{Gas\ Unc.^2 + MFC\ Unc.^2 + Cal.Eff.^2} \qquad \text{Eq. A2}$$

$$Gas\ Unc.^2 = Acetone^2 + NO_x^2 + Zero\ Air^2 \qquad \text{Eq. A2.1}$$

$$Acetone = Acetone\ Uncertainty = 0.05$$

$$NO_x = NO_x\ Uncertainty = 0.02$$

$$Zero\ Air = Zero\ Air\ Uncertainty = See\ Text$$

$$MFC\ Unc.^2 = A.MFC^2 + N.MFC^2 + Z.MFC^2 \qquad \text{Eq. A2.2}$$

$$A.MFC = Acetone\ MFC\ Unc. = 0.01$$

$$N.MFC = NO_x\ MFC\ Unc. = 0.03$$

$$Z.MFC = Zero\ Air\ MFC\ Unc. = 0.06$$

The precision of the in situ point calibrations was calculated as the relative standard deviation of the point calibrations.

Table A1: The standard deviation (Stdev), mean, and relative standard deviation (RSD) of the campaign-wide PAN point calibrations for both columns and both the "clean" and "noisy" periods. The units are Area units.

	"Clean"			"Noisy"		
	Stdev	Mean	RSD	Stdev	Mean	RSD
Column 1	1.82	32.86	0.06	1.67	58.06	0.03
Column 2	1.57	35.30	0.04	1.92	59.51	0.03

The final instrument uncertainty was calculated using Equation A3, where $Precision^2$ is given above as the relative standard deviation. $PAN\ GC\ Unc.$ was 0.11 for July and 0.10 for August in column 1, and 0.10 for July and 0.10 for August in column 2.

$$PAN\ GC\ Unc. = \sqrt{Calibrator\ Unc.^2 + Precision^2} \qquad \text{Eq. A3}$$

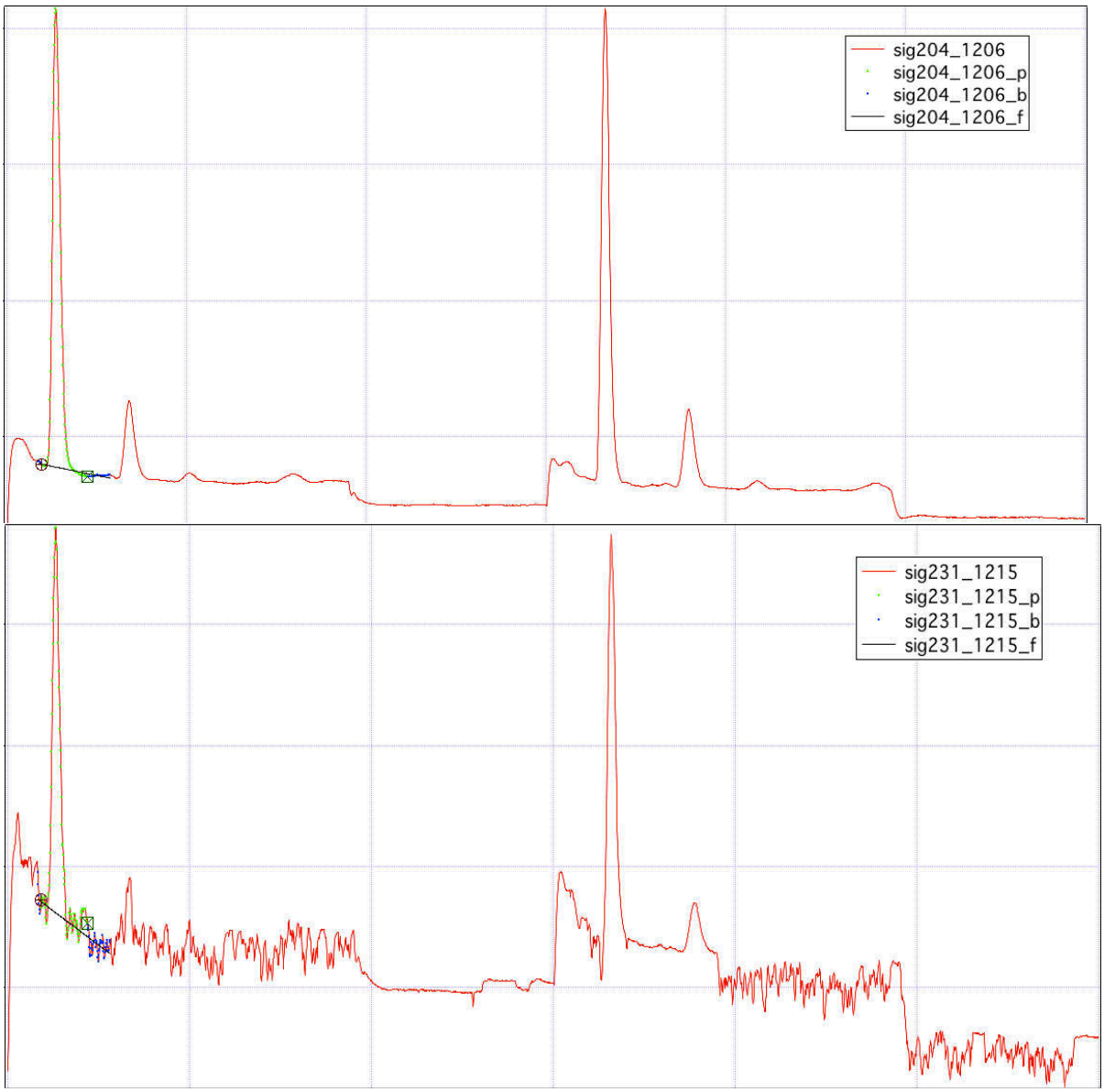

Figure A6: Example of "clean" and "noisy" chromatograms. For "clean" chromatograms, the peaks can be easily distinguished from the baseline and are easy to integrate. For "noisy" chromatograms, peaks cannot be easily distinguished from the baseline. Note, MPAN is not available for "noisy" periods (August). The LOD for PAN during the "clean" period is 2 pptv and during the "noisy" period is 20 pptv.

LODs were calculated with Equation A4, where σ is the standard deviation of an example "clean" or "noisy" baseline (in Hz), $\frac{A}{H}$ is the ratio of peak area to peak height (Area units/Hz), and α is the conversion factor between area and mixing ratio in pptv (pptv/Area units).

$$LOD = 3\sigma \frac{A}{H} \alpha \qquad \text{Eq. A4}$$

Table A2: 3σ for the "clean" and "noisy" baselines, $\frac{A}{H}$ for both columns, and α for both columns.

	"Clean"			"Noisy"		
	3σ	$\frac{A}{H}$	α	3σ	$\frac{A}{H}$	α
Column 1	0.032	4.73	11	0.41	4.73	11
Column 2	0.032	4.91	9.8	0.41	4.91	9.8

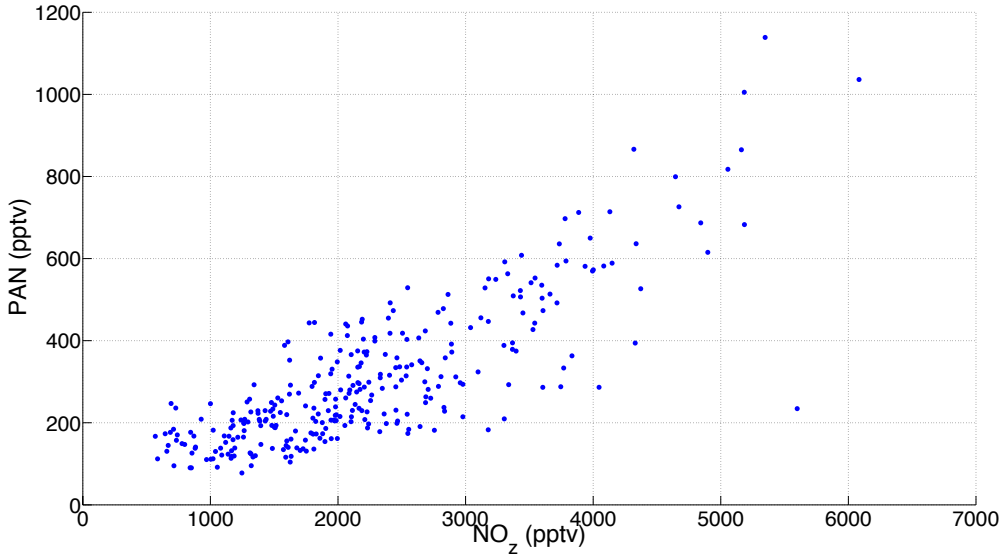

Figure A7: Daytime (6 MDT to 18 MDT) hourly mean PAN versus NO_z values for the entire campaign.

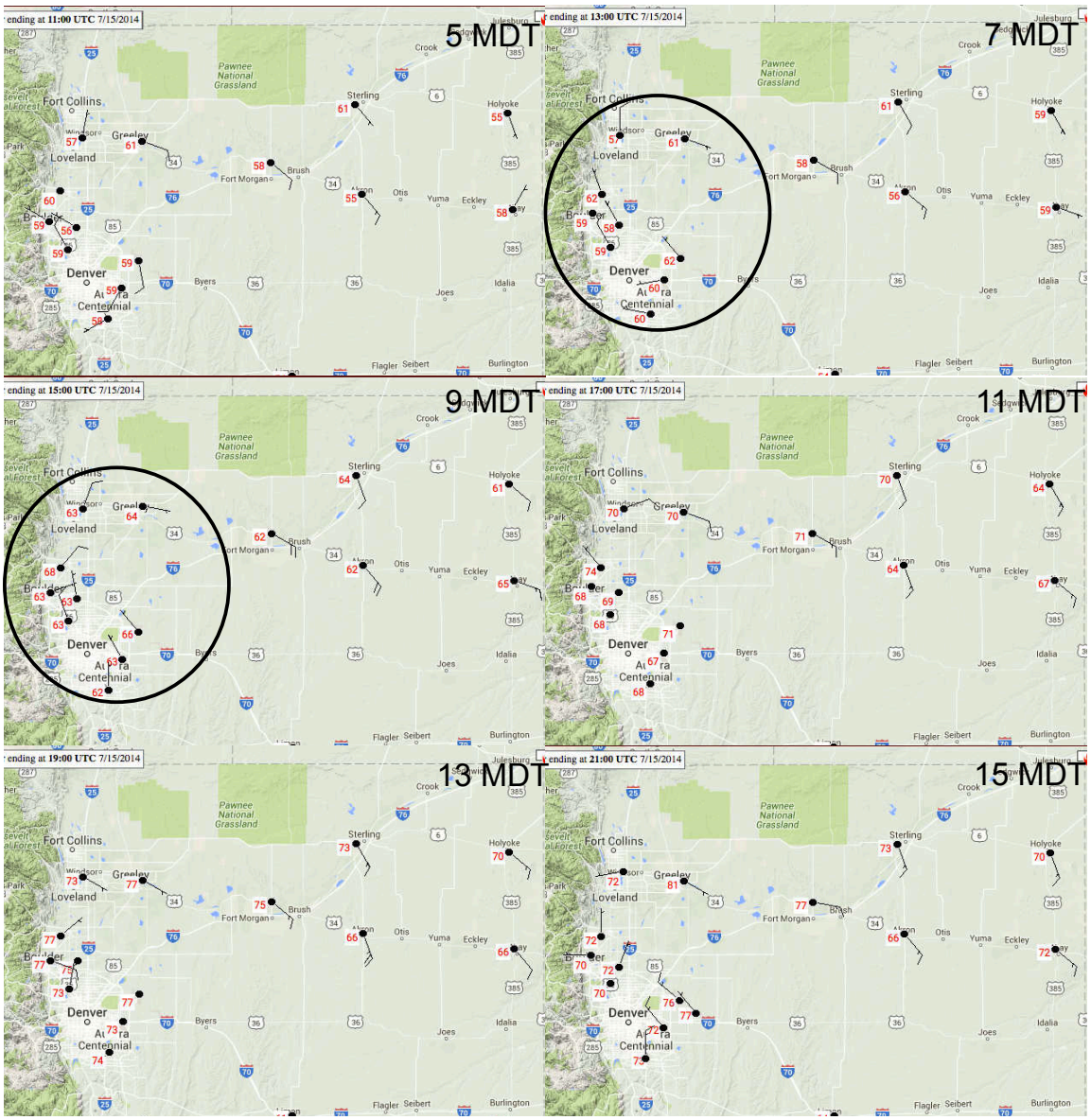

Figure A8: Examples of Denver Cyclone Event from The University of Utah MesoWest website (http://mesowest.utah.edu/cgi-bin/droman/mesomap.cgi?state=CO&rawsflag=3). Regional winds at 5, 7, 9, 11, 13, and 15 MDT (11, 13, 15, 17, 19, and 21 UTC) on 7/15/14 (a high PAN day). Notice the clear "gyre" of winds present at 7 and 9 MDT.

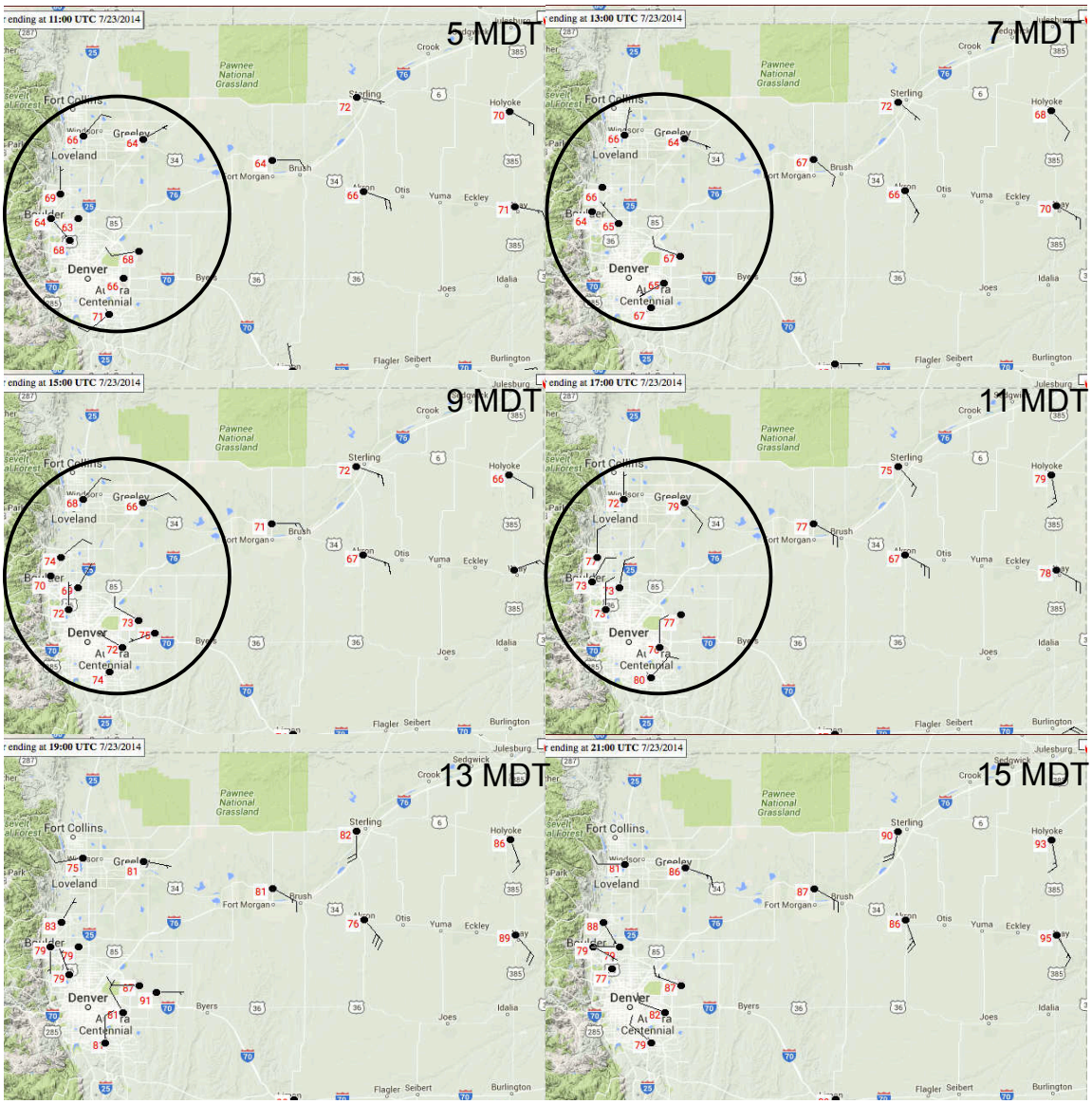

Figure A9: Regional winds for the same times as above on 7/23/14 (high PAN day). Note the clear "gyre" present between 5 and 11 MDT.

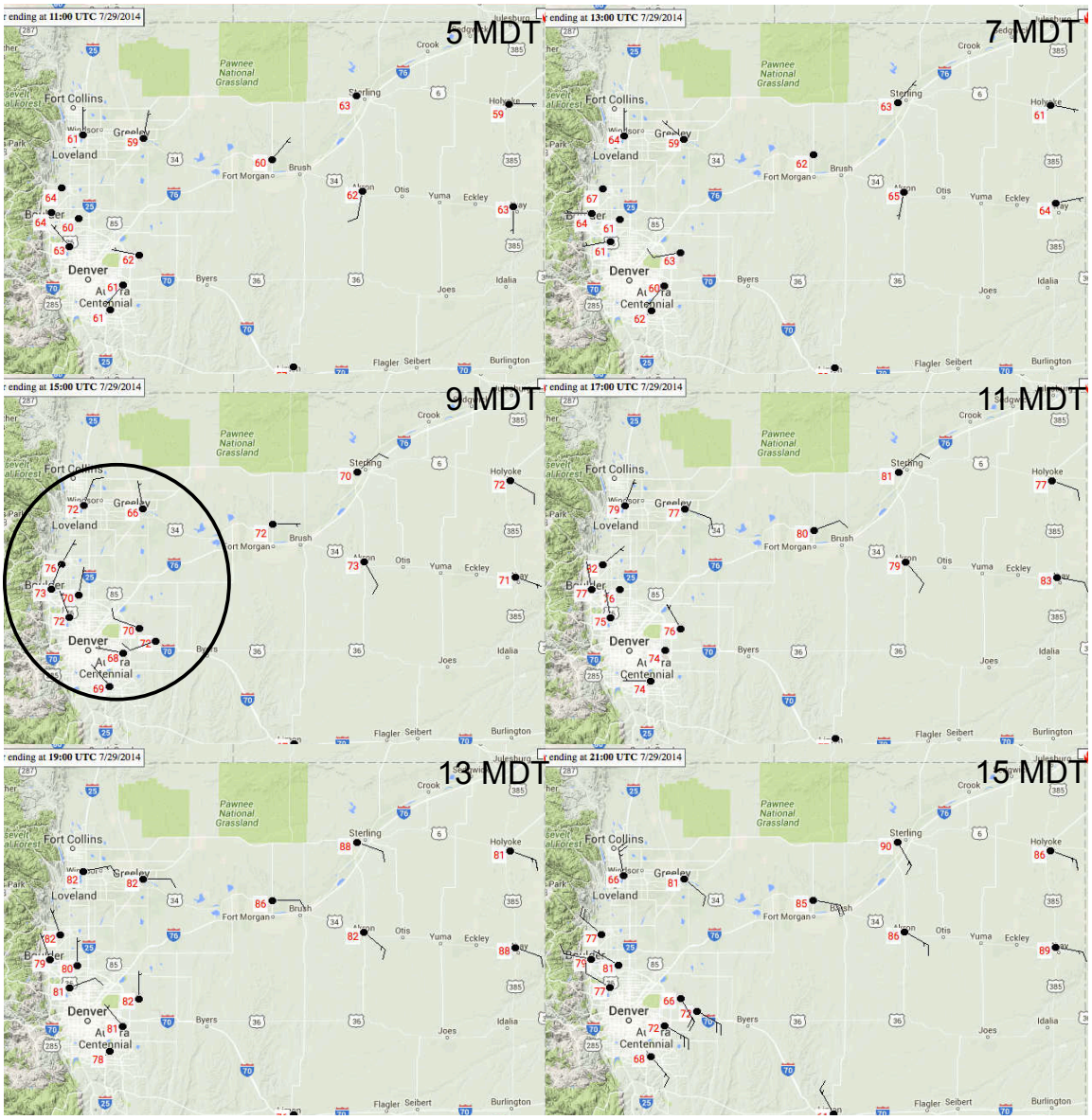

Figure A10: Regional winds for the same times as above on 7/29/14 (high PAN day). Note the clear "gyre" at 9 MDT.

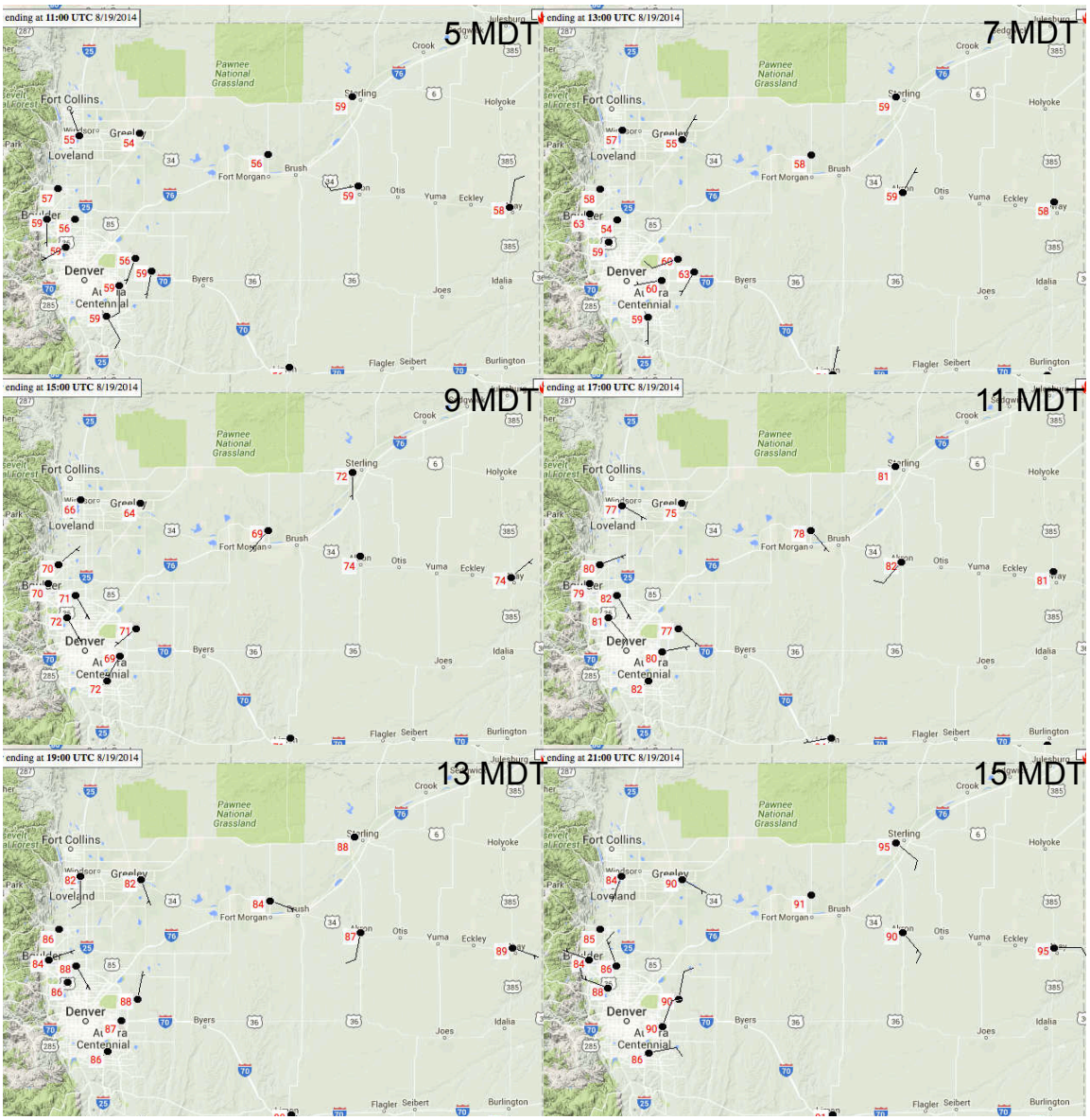

Figure A11: Regional winds for the same times as above on 8/19/14 (high PAN day). Note the lack of the characteristic "gyre" described above.

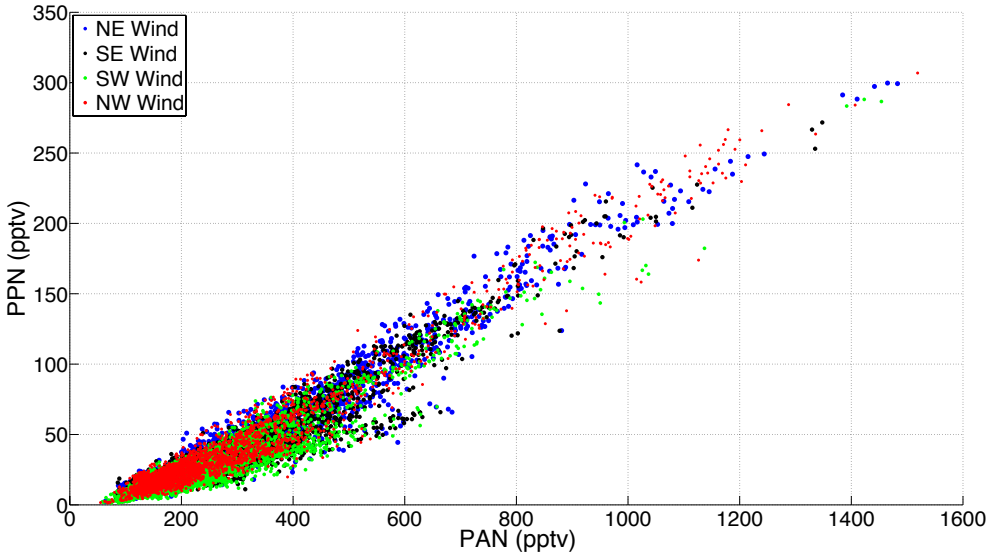

Figure A12: Simultaneous 5-minute point PPN versus PAN for the entire campaign subset by wind direction. Wind bins break at multiples of 90°.

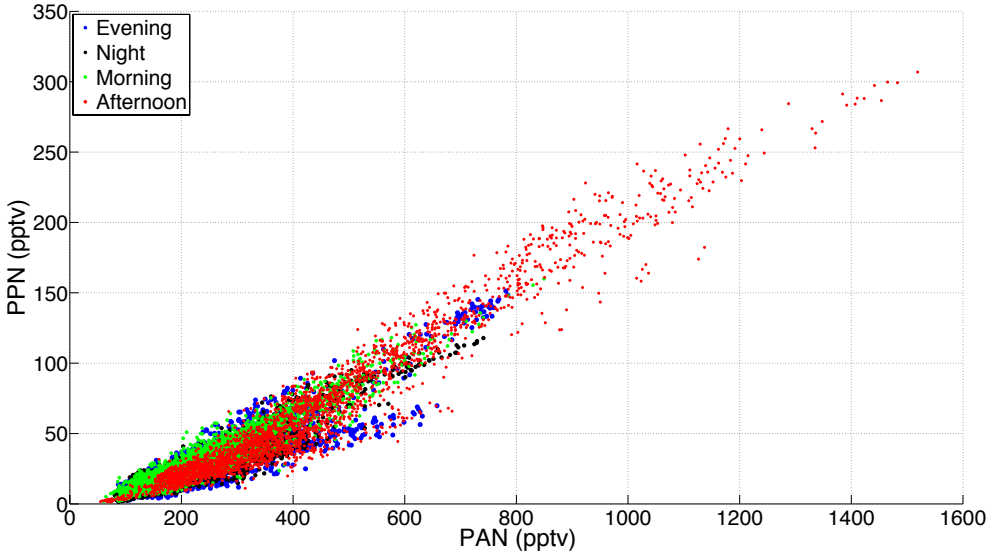

Figure A13: Simultaneous 5-minute point PPN versus PAN for the entire campaign subset by time of day. Evening is 18 MDT to 24 MDT, night is 0 MDT to 6 MDT, morning is 6 MDT to 12 MDT, and afternoon is 12 MDT to 18 MDT.

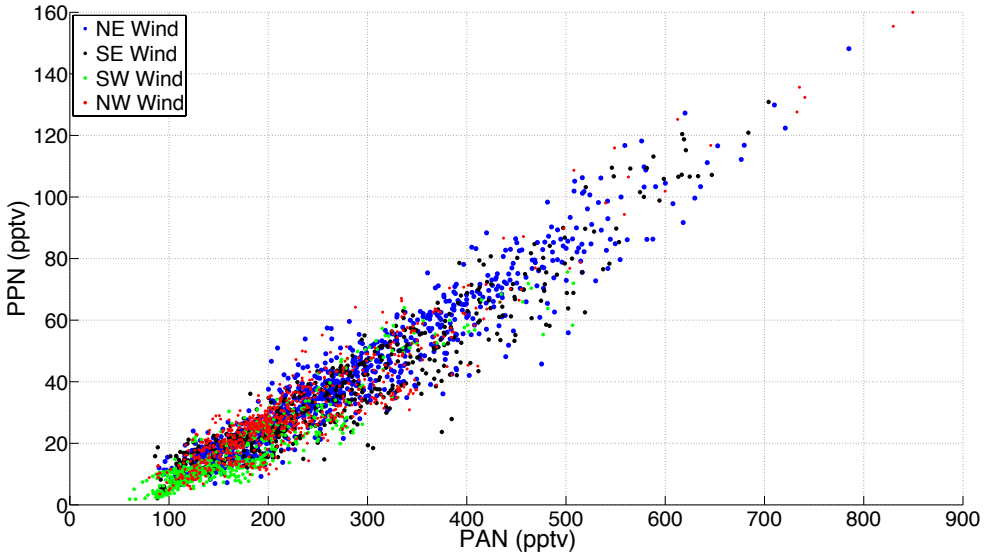

Figure A14: Simultaneous 5-minute point PPN versus PAN for only morning times (6 MDT to 12 MDT) subset by wind direction. Wind bins are the same as above.

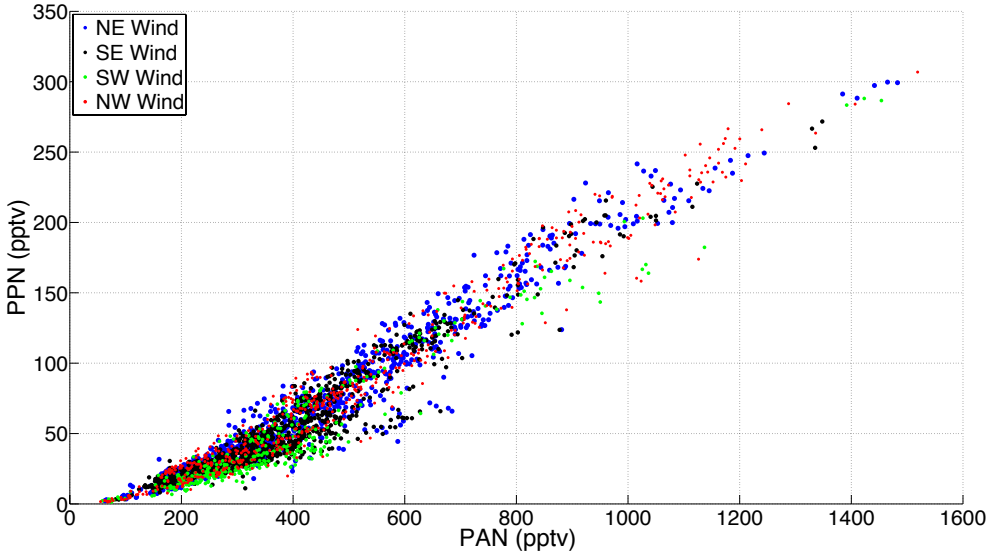

Figure A15: Simultaneous 5-minute point PPN versus PAN for only afternoon times (12 MDT to 18 MDT) subset by wind direction. Wind bins are the same as above.

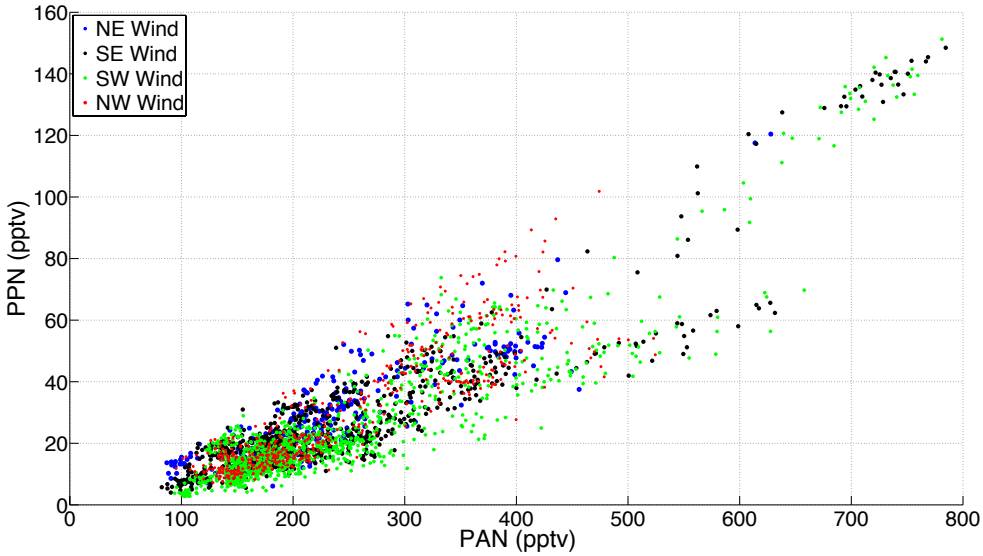

Figure A16: Simultaneous 5-minute point PPN versus PAN for only evening times (18 MDT to 24 MDT) subset by wind direction. Wind bins are the same as above.

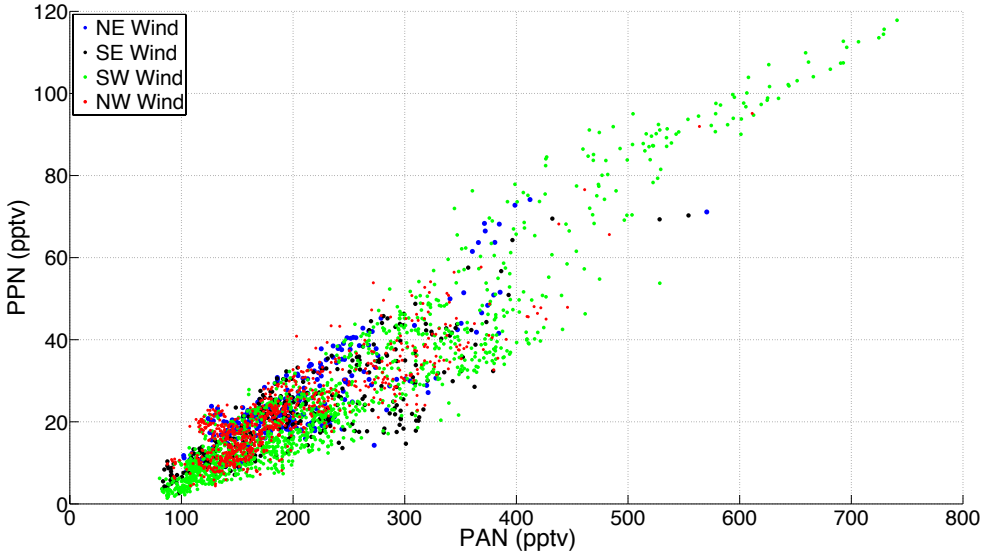

Figure A17: Simultaneous 5-minute point PPN versus PAN for only night times (0 MDT to 6 MDT) subset by wind direction. Wind bins are the same as above.

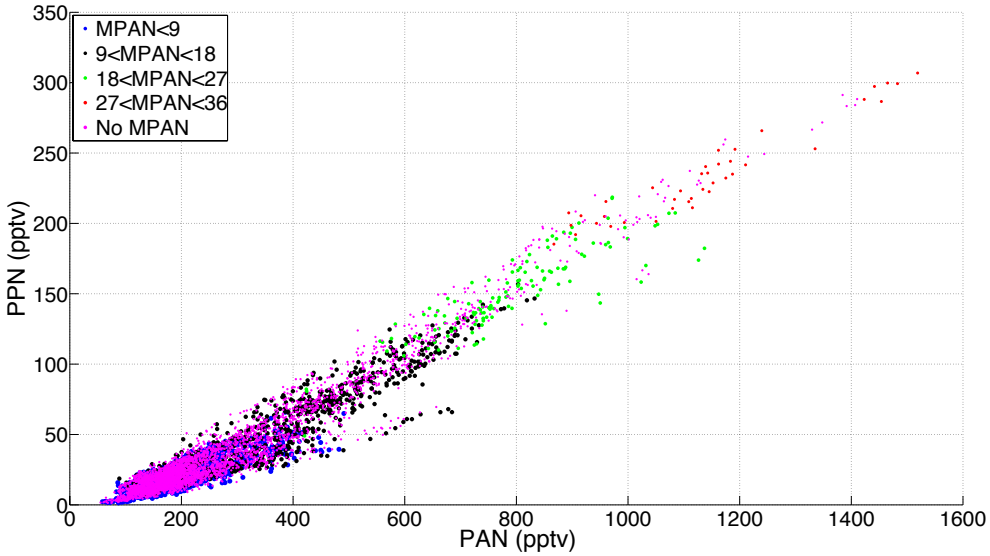

Figure A18: Simultaneous 5-minute point PPN versus PAN for the entire campaign subset by MPAN abundance.

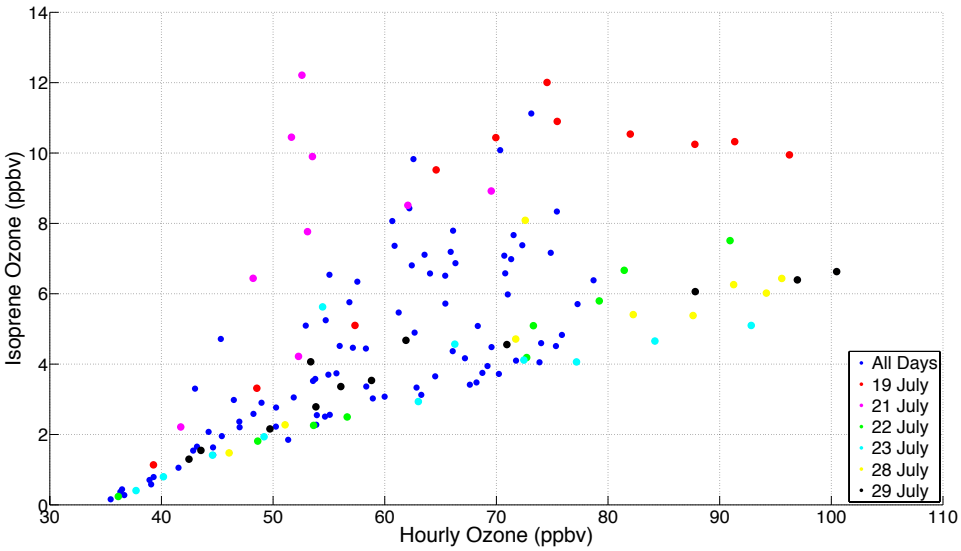

Figure A19: Estimated O_3 from biogenic VOCs (isoprene ozone) calculated using Equation 2 (see thesis document) versus hourly averaged measured O_3. Background O_3 is set to 35 ppbv for this calculation.

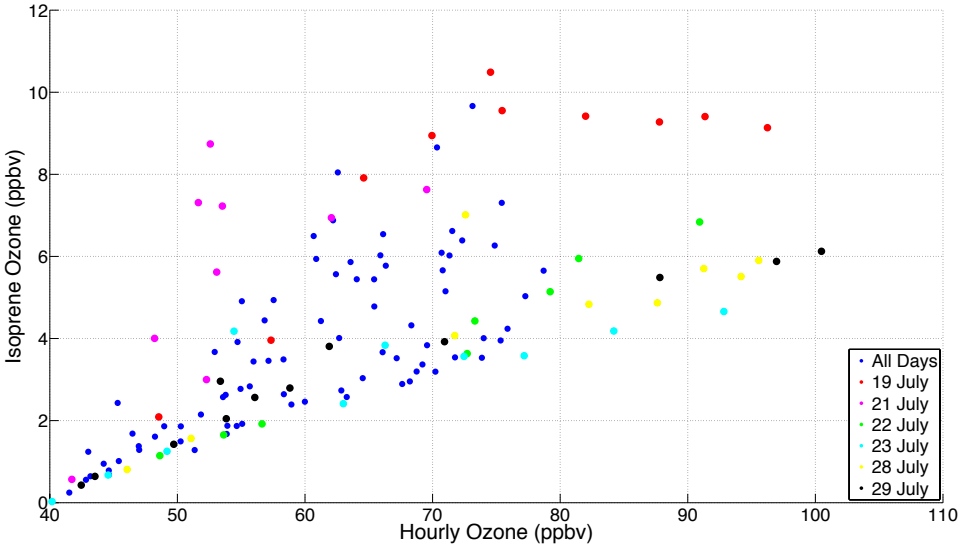

Figure A20: Estimated O_3 from biogenic VOCs (isoprene ozone) calculated using Equation 2 (see thesis document) versus hourly averaged measured O_3. Background O_3 is set to 40 ppbv for this calculation.

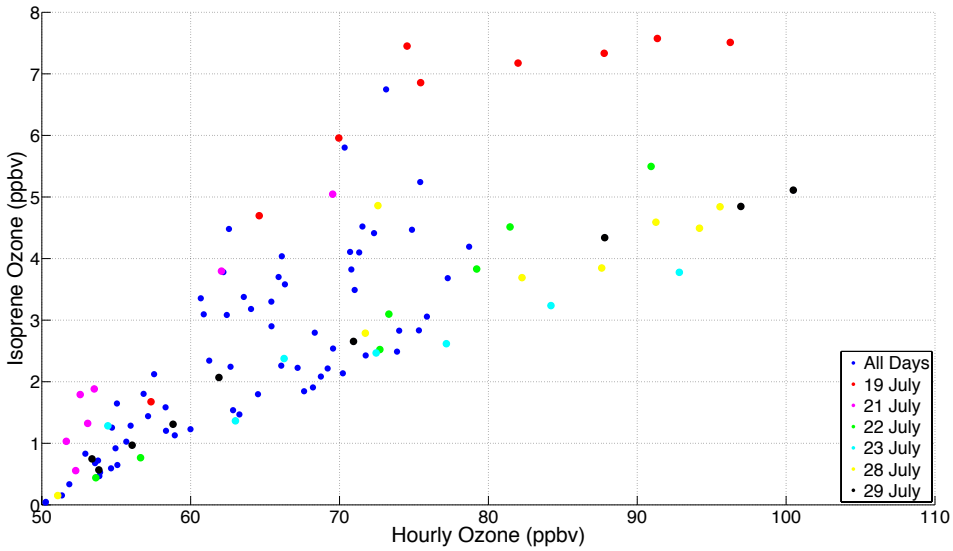

Figure A21: Estimated O_3 from biogenic VOCs (isoprene ozone) calculated using Equation 2 (see thesis document) versus hourly averaged measured O_3. Background O_3 is set to 50 ppbv for this calculation.

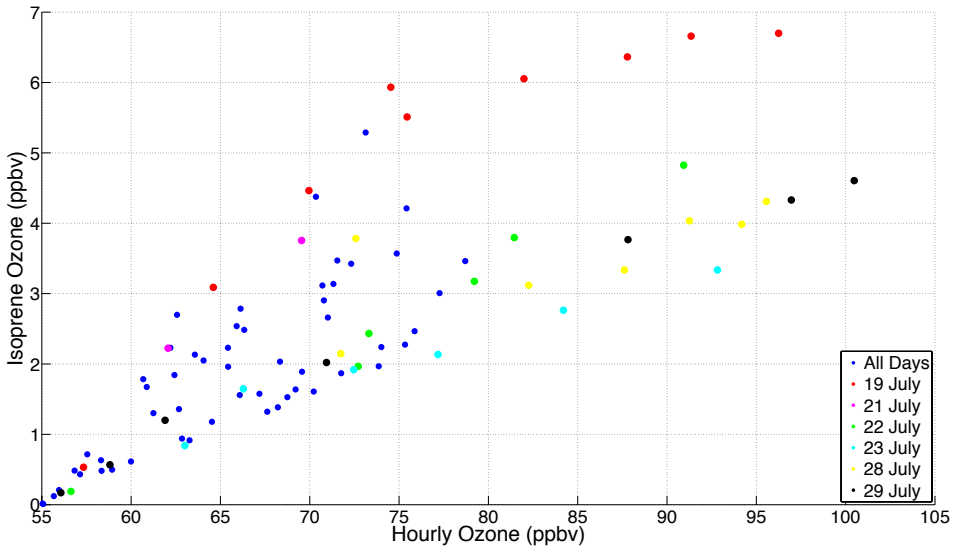

Figure A22: Estimated O_3 from biogenic VOCs (isoprene ozone) calculated using Equation 2 (see thesis document) versus hourly averaged measured O_3. Background O_3 is set to 55 ppbv for this calculation.

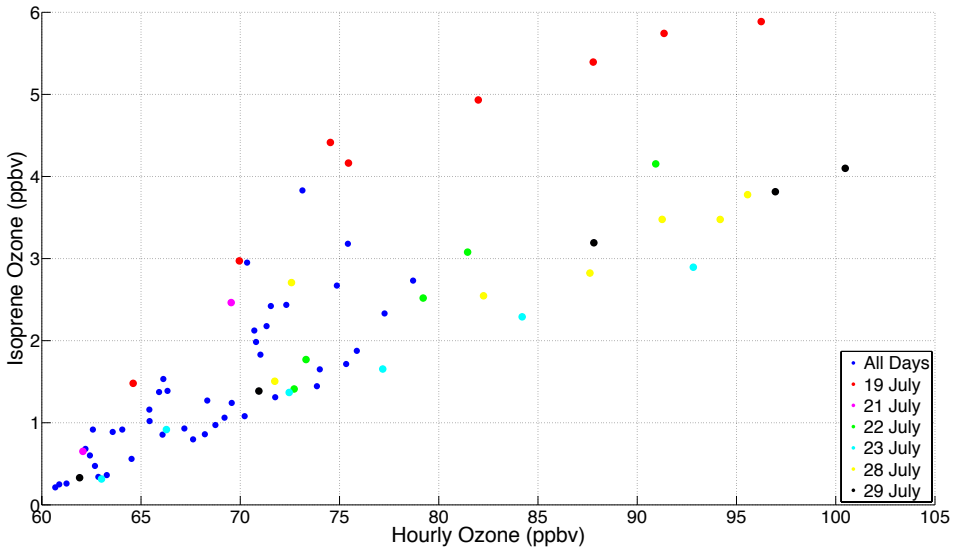

Figure A23: Estimated O_3 from biogenic VOCs (isoprene ozone) calculated using Equation 2 (see thesis document) versus hourly averaged measured O_3. Background O_3 is set to 60 ppbv for this calculation.

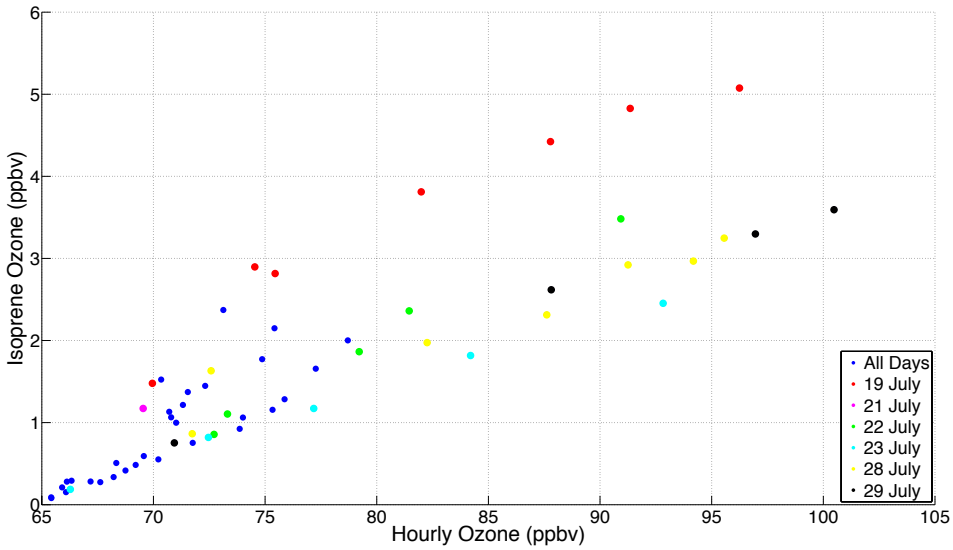

Figure A24: Estimated O_3 from biogenic VOCs (isoprene ozone) calculated using Equation 2 (see thesis document) versus hourly averaged measured O_3. Background O_3 is set to 65 ppbv for this calculation.

IGOR Integration Procedure:

Running IGOR Normally

1. Open IGOR
2. File -> Open File -> Procedure
    a. Open 5min_chroms.ipf
3. This is a new IGOR experiment, so you will need to create new global variables. **To do this, you copy the following into the command line, do not copy the "//":**
    a. variable /g BeginPeak, EndPeak, BeginBackground, EndBackground
    b. variable /g PeakArea, PeakCurveArea, BackgroundArea
    c. variable /g ddd, hh, mm
    d. variable /g FitType, PeakType, PeakFound
4. You may need to compile 5min_chroms.ipf. You do this with the compile button on the bottom of the window.
5. Macros -> LoadChromatFiles99, and choose the folder that has the data in it.
    a. Now you can see the chromatograms in the data browser.
    b. Data -> DataBrowser
    c. Macros -> DoManyChromPAN
    d. Macros -> DoManyChromPAN2
    e. Macros -> DoManyChromPPN
    f. Macros -> DoManyChromPeak1 (PPN2)
6. Copy data out of DataBrowser. The waves of interest are Chrom_time, PAN_area, and PAN2_area

Checking Chromatograms/Manually Integrating

After Step 5 of Normal IGOR use:

1. Macros -> Redo_one_chrom_99
    a. Select signal wave (time)
    b. Select Peak (PAN, PPN, MPAN, PAN2, etc.)
    c. Continue
    d. After adjusting PeakCursors
        i. Click "change background cursors"
        ii. This changes the "background" for integration
    e. Move PeakCursors for actual integration Start and Stop points
        i. Click "change peak cursors"
    f. Click "recalculate area"
2. To save into DataBrowser PeakAreas:
    a. Choose "Linear"
    b. Choose corresponding peak
    c. Save
3. You can do this and then pull the final PeakArea list from the DataBrowser at the end. However, if at any point during this you accidentally hit "DoManyChromX" all manual integrations will be rewritten. And it happens more often than you would think.
4. One work around is to copy the entire PeakArea list into an excel sheet, with the corresponding time in another column. Then manually change the area and update the peak areas in the excel sheet as you go.

To Adjust Peak Search and Auto Integration Parameters

1. When optimized, automatic integrations through IGOR are awesome! You literally follow steps 1-6 above, call it good and move on to the next day. Sanity-checking one or two chromatograms manually in the process to make sure things are running smoothly.
2. To optimize:
    a. After step 3 of normal IGOR running.
    b. In the 5min_chroms.ipf file, towards the bottom the different macros for the various DoManyChromXs are defined.
    c. Scroll to the macro of the compound you are working on.
        i. "variable secsPANbegins" and "variable secsPANends" tell IGOR look between here and here for the peak maximum. You usually don't need to change these.
        ii. "variable BeginPeakDelta" and "variable EndPeakDelta" are the start and stop points of the integration.
        iii. "variable BeginBkgrndDelta" and "EndBkgrndDelta" are the background start and stop points. These all always be greater than the corresponding peak integration start/stop points.
    d. Compile the 5min_chroms.ipf procedure (see above Step 4).
3. Follow normal IGOR use.
4. To quickly check your new peak search/peak integrations parameters, run the macros for the corresponding compound, then redo a random peak. If you don't like it, readjust your parameters, checking after each until you like what you see! If you like it, check a few more chromatograms, if they all seem okay, you are set! The instrument is incredibly stable if we don't mess with it, so usually once you are optimized you can "plug and chug." Occasionally though things will change, at which point another optimization may be in order!
5. ***Note***
    a. A combination of IGOR and an integration program written by Steven Brey was used to integrate the peak areas.
6. Raw text files are located on ozone, in the following directory:
    a. /fischer-scratch/group-share/PANData_BAO.
7. Png images of chromatograms and integrations performed by Steven Brey are located on ozone, in the following directory:
    a. /fischer-scratch/group-share/PANData_BAO/AutomaticAnalysis

Data Finalization:
Below is the MatLab code ('BAO_PAN_Data_finalization_7_21_15.m') that was used to finalize the raw peak areas and output .csv files that became the final ICARTT files. After all the desired peaks were integrated, a new .csv file ('BAO_PAN_Data_for_import_7_21_15.csv') was created that organized all peak areas. The table below (A1) provides the first few lines of the table highlighting its organizational scheme and relevant formats. The time formats are key for the MatLab code to work.

Table A1: Example of first 9 rows of 'BAO_PAN_Data_for_import_7_21_15.csv.' 'PAN1_Cal_Flag' and 'PAN2_Cal_Flag' mark in situ calibrations so the MatLab code can remove them.

Date1	Time1	PAN1_Area	PAN1_Cal_Flag	Date2	Time2	PAN2_Area	PAN2_Cal_Flag	PPN1_Area	PPN2_Area	MPAN1_Are	MPAN2_Are
7/9/14	0:03:00	16.1883	0	7/9/14	0:08:00	28.818	1	2.43131	-0.0526416	-9999	-9999
7/9/14	0:13:00	15.4172	0	7/9/14	0:18:00	17.8375	0	2.45178	2.65833	0.633907	-9999
7/9/14	0:23:00	15.2827	0	7/9/14	0:28:00	17.4462	0	2.40229	2.47443	0.554417	-9999
7/9/14	0:33:00	26.5017	1	7/9/14	0:38:00	13.7225	0	-0.0196989	2.62157	-0.0695209	-9999
7/9/14	0:43:00	15.2389	0	7/9/14	0:48:00	17.6182	0	2.46719	2.6317	0.706966	-9999
7/9/14	0:53:00	14.5986	0	7/9/14	0:58:00	17.8315	0	2.2935	2.52689	0.620203	-9999
7/9/14	1:03:00	15.3734	0	7/9/14	1:08:00	29.537	1	2.37405	0.0801861	-9999	-9999
7/9/14	1:13:00	14.9769	0	7/9/14	1:18:00	17.1368	0	2.41057	2.44481	-9999	-9999

```
clear all;
close all;
clc;

%% Import data from text file.
% Script for importing data from the following text file:
%
%    /Users/efischer/Documents/Current
%    Projects/BAO_Data/PANData/Finalizing_PAN_Data/BAO_PAN_Data_for_import_1_5_15.csv
%
% To extend the code to different selected data or a different text file,
% generate a function instead of a script.

% Auto-generated by MATLAB on 2015/01/05 11:20:38

%% Initialize variables.
filename =
'/Users/jzaragoza/Documents/Research/PAN_GC/PAN_GC_Integration/BAO_PAN_Data_for_import_7_21_15.csv'
;
delimiter = ',';
startRow = 2;

%% Read columns of data as strings:
% For more information, see the TEXTSCAN documentation.
formatSpec = '%s%s%s%s%s%s%s%s%s%s%s%s%s%[^\n\r]';

%% Open the text file.
fileID = fopen(filename,'r');

%% Read columns of data according to format string.
% This call is based on the structure of the file used to generate this
% code. If an error occurs for a different file, try regenerating the code
% from the Import Tool.
```

```
dataArray = textscan(fileID, formatSpec, 'Delimiter', delimiter, 'HeaderLines' ,startRow-1, 'ReturnOnError', false);

%% Close the text file.
fclose(fileID);

%% Convert the contents of columns containing numeric strings to numbers.
% Replace non-numeric strings with NaN.
raw = repmat({''},length(dataArray{1}),length(dataArray)-1);
for col=1:length(dataArray)-1
    raw(1:length(dataArray{col}),col) = dataArray{col};
end
numericData = NaN(size(dataArray{1},1),size(dataArray,2));

for col=[3,4,7,8,9,10,11,12]
    % Converts strings in the input cell array to numbers. Replaced non-numeric
    % strings with NaN.
    rawData = dataArray{col};
    for row=1:size(rawData, 1);
        % Create a regular expression to detect and remove non-numeric prefixes and
        % suffixes.
        regexstr = '(?<prefix>.*?)(?<numbers>([-]*(\d+[\,]*)+[\.]{0,1}\d*[eEdD]{0,1}[-+]*\d*[i]{0,1})|([-
]*(\d+[\,]*)*[\.]{1,1}\d+[eEdD]{0,1}[-+]*\d*[i]{0,1}))(?<suffix>.*)';
        try
            result = regexp(rawData{row}, regexstr, 'names');
            numbers = result.numbers;

            % Detected commas in non-thousand locations.
            invalidThousandsSeparator = false;
            if any(numbers==',');
                thousandsRegExp = '^\d+?(\,\d{3})*\.{0,1}\d*$';
                if isempty(regexp(thousandsRegExp, ',', 'once'));
                    numbers = NaN;
                    invalidThousandsSeparator = true;
                end
            end
            % Convert numeric strings to numbers.
            if ~invalidThousandsSeparator;
                numbers = textscan(strrep(numbers, ',', ''), '%f');
                numericData(row, col) = numbers{1};
                raw{row, col} = numbers{1};
            end
        catch me
        end
    end
end

%% Split data into numeric and cell columns.
rawNumericColumns = raw(:, [3,4,7,8,9,10,11,12]);
rawCellColumns = raw(:, [1,2,5,6]);


%% Replace non-numeric cells with NaN
R = cellfun(@(x) ~isnumeric(x) && ~islogical(x),rawNumericColumns); % Find non-numeric cells
rawNumericColumns(R) = {NaN}; % Replace non-numeric cells
```

```
%% Allocate imported array to column variable names
Date1 = rawCellColumns(:, 1);
Time1 = rawCellColumns(:, 2);
PAN1_Area = cell2mat(rawNumericColumns(:, 1));
PAN1_Cal_Flag = cell2mat(rawNumericColumns(:, 2));
Date2 = rawCellColumns(:, 3);

Time2 = rawCellColumns(:, 4);
PAN2_Area = cell2mat(rawNumericColumns(:, 3));
PAN2_Cal_Flag = cell2mat(rawNumericColumns(:, 4));
PPN1_Area = cell2mat(rawNumericColumns(:, 5));
PPN2_Area = cell2mat(rawNumericColumns(:, 6));
MPAN1_Area = cell2mat(rawNumericColumns(:, 7));
MPAN2_Area = cell2mat(rawNumericColumns(:, 8));

clearvars R ans col dataArray delimiter fileID formatSpec numbers numericData raw rawCellColumns rawData
rawNumericColumns regextr result row startRow invalidThousandsSeparator me regexstr
%% Now get the dates in the right format

% % Deal with Dates - Get Dates into Matlab Date format
time1_matlab_local = datenum(Time1,'HH:MM:SS');
time2_matlab_local = datenum(Time2,'HH:MM:SS');
date1_matlab_local = datenum(Date1, 'yyyy/mm/dd');
date2_matlab_local = datenum(Date2, 'yyyy/mm/dd');
jannum = datenum(str2double('2015'), 1, 1);
sample_time_1_matlab_local = time1_matlab_local + date1_matlab_local - jannum;
sample_time_2_matlab_local = time2_matlab_local + date2_matlab_local - jannum;
%% Now separate the calibrations from the actual data

data_index_column_1 = find(PAN1_Cal_Flag == 0);
data_index_column_2 = find(PAN2_Cal_Flag == 0);
cal_index_column_1 = find(PAN1_Cal_Flag == 1);
cal_index_column_2 = find(PAN2_Cal_Flag == 1);

Data_PAN1_Area = PAN1_Area(data_index_column_1);
PAN1_Cals = PAN1_Area(cal_index_column_1);
Data_PAN2_Area = PAN2_Area(data_index_column_2);
PAN2_Cals = PAN2_Area(cal_index_column_2);
PPN1_Area = PPN1_Area(data_index_column_1);
PPN2_Area = PPN2_Area(data_index_column_2);
MPAN1_Area = MPAN1_Area(data_index_column_1);
MPAN2_Area = MPAN2_Area(data_index_column_2);
sample_time_1_matlab_local_PAN1_data = sample_time_1_matlab_local(data_index_column_1);
sample_time_2_matlab_local_PAN2_data = sample_time_2_matlab_local(data_index_column_2);
cal_time_1_matlab_local_PAN1_data = sample_time_1_matlab_local(cal_index_column_1);
cal_time_2_matlab_local_PAN2_data = sample_time_2_matlab_local(cal_index_column_2);

% figure;
% plot(sample_time_1_matlab_local_PAN1_data, Data_PAN1_Area);
% hold on;
% datetick('x',0); ylim([0 200]);

% figure;
```

```
% plot(cal_time_1_matlab_local_PAN1_data, PAN1_Cals);
% hold on;
% datetick('x',0); ylim([0 200]);
%% Apply conversion to get PAN mixing ratio from peak area
% note changes in both calibration gas concentrations and sample pressure
% that occurred. So the same calibration factor is not applied throughout
% only convert when you do not have a -9999 or a -8888
% Note different response factor for column 1 and column 2
% higher sample pressure was set on 8/10/14 starting with sample at 18:16
% local time.  This is row 4671.

response_index_PAN1 = find(Data_PAN1_Area > -7777);

PAN1_pptv = Data_PAN1_Area;
for x = 1: 4670
   if PAN1_Area(x) > -8888
      PAN1_pptv(x) = Data_PAN1_Area(x)*0.011*1000;
   else
      PAN1_pptv(x) = Data_PAN1_Area(x);
   end
end


for x = 4671: length(Data_PAN1_Area)
   if Data_PAN1_Area(x) > -8888
      PAN1_pptv(x) = Data_PAN1_Area(x)*0.011*1000*(57.9587/48.96742);
   else
      PAN1_pptv(x) = Data_PAN1_Area(x);
   end
end

PAN2_pptv = Data_PAN2_Area;
for x = 1: 4670
   if PAN2_Area(x) > -8888
      PAN2_pptv(x) = Data_PAN2_Area(x)*0.0098*1000;
   else
      PAN2_pptv(x) = Data_PAN2_Area(x);
   end
end


for x = 4671: length(Data_PAN2_Area)
   if Data_PAN2_Area(x) > -8888
      PAN2_pptv(x) = Data_PAN2_Area(x)*0.0098*1000*(57.9587/48.96742);
   else
      PAN2_pptv(x) = Data_PAN2_Area(x);
   end
end

PPN1_pptv = PPN1_Area;
for x = 1: 4670
   if PPN1_Area(x) > -8888
      PPN1_pptv(x) = PPN1_Area(x)*0.011*0.9*1000;
   else
```

```
      PPN1_pptv(x) = PPN1_Area(x);
   end
end



for x = 4671: length(PPN1_Area)
   if PPN1_Area(x) > -8888
      PPN1_pptv(x) = PPN1_Area(x)*0.011*0.9*1000*(57.9587/48.96742);
   else
      PPN1_pptv(x) = PPN1_Area(x);
   end
end

PPN2_pptv = PPN2_Area;
for x = 1: 4670;
   if PPN2_Area(x) > -8888;
      PPN2_pptv(x) = PPN2_Area(x)*0.0098*0.9*1000;
   else
      PPN2_pptv(x) = PPN2_Area(x);
   end
end



for x = 4671: length(PPN2_Area);
   if PPN2_Area(x) > -8888;
      PPN2_pptv(x) = PPN2_Area(x)*0.0098*0.9*1000*(57.9587/48.96742);
   else
      PPN2_pptv(x) = PPN2_Area(x);
   end
end

MPAN1_pptv = MPAN1_Area;
for x = 1: 4670
   if MPAN1_Area(x) > -8888
      MPAN1_pptv(x) = MPAN1_Area(x)*0.011*0.64*1000;
   else
      MPAN1_pptv(x) = MPAN1_Area(x);
   end
end



for x = 4671: length(MPAN1_Area)
   if MPAN1_Area(x) > -8888
      MPAN1_pptv(x) = MPAN1_Area(x)*0.011*0.64*1000*(57.9587/48.96742);
   else
      MPAN1_pptv(x) = MPAN1_Area(x);
   end
end

MPAN2_pptv = MPAN2_Area;
for x = 1: 4670;
   if MPAN2_Area(x) > -8888;
```

```
    MPAN2_pptv(x) = MPAN2_Area(x)*0.0098*0.64*1000;
  else
    MPAN2_pptv(x) = MPAN2_Area(x);
  end
end


for x = 4671: length(MPAN2_Area);
  if MPAN2_Area(x) > -8888;
    MPAN2_pptv(x) = MPAN2_Area(x)*0.0098*0.64*1000*(57.9587/48.96742);
  else
    MPAN2_pptv(x) = MPAN2_Area(x);
  end
end



%% Now we need to combine PAN1 and PAN2, and PPN1 and PPN2, and MPAN1 and MPAN2, and the two time
bases into 4 vectors instead of 8

% Combine vectors
PAN_pptv = vertcat(PAN1_pptv, PAN2_pptv);
PPN_pptv = vertcat(PPN1_pptv, PPN2_pptv);
MPAN_pptv = vertcat(MPAN1_pptv, MPAN2_pptv);
sample_time_local_matlab = vertcat(sample_time_1_matlab_local_PAN1_data,
sample_time_2_matlab_local_PAN2_data);
% Now need to get the time in UTC rather than local time.
% UTC is local time + 6 hours
for x = 1: length(sample_time_local_matlab);
  sample_time_UTC_matlab(x) = addtodate(sample_time_local_matlab(x), 6, 'hour');
end
unsorted_data = horzcat(sample_time_UTC_matlab', PAN_pptv, PPN_pptv, MPAN_pptv);
sorted_data = sortrows(unsorted_data, 1);
%
% %Figures for Checking
% figure;
% plot(sample_time_1_matlab_local_PAN1_data, PAN1_pptv)
% hold on;
% datetick('x',0); ylim([0 1500]);
%
% figure;
% plot(sample_time_2_matlab_local_PAN2_data, PAN2_pptv)
% hold on;
% datetick('x',0); ylim([0 1500]);
%
% %
% figure;
% plot(sorted_data(:,1), sorted_data(:,2));
% hold on;
% datetick('x',0); ylim([0 1500]);

%% Separate into individual days from July 9 to July 31 and August 1 to August 22 based on the day.
[Y, M, D, H, MN, S] = datevec(sorted_data(:,1));
%Y = Y', D = D', M = M', H = H'; MN = MN', S = S';
```

```
% July is rows 1:6360 - need to check this if Jake give a new raw peak area
% file.

% Make a column that is UTC seconds for each day from 00UTC. This will be
% used to slot the PAN measurements into the right time in the ICARTT data
% files.

UTC_seconds = S + MN*60 + H*60*60;

sorted_data_with_date = horzcat(D, H, MN, S, UTC_seconds, sorted_data);
sorted_data_July = sorted_data_with_date(1:6361, :);
sorted_data_August = sorted_data_with_date(6361:length(sorted_data_with_date), :);
Days_July = arrayfun(@(x) sorted_data_July(sorted_data_July(:,1) == x, :), unique(sorted_data_July(:,1)),
'uniformoutput', false);
Days_August = arrayfun(@(x) sorted_data_August(sorted_data_August(:,1) == x, :),
unique(sorted_data_August(:,1)), 'uniformoutput', false);

%% Now put the rows for each day into the right rows for a ICARRT text file with the first column as every second
of UTC time in a given day

utc_seconds = [0:1:86399]';

% Do July and August Separately since they are in Separate Cell Arrays at
% this point.
for z = 2:24; % Not sure why the first cell array in July_Days is strange
PAN_final = -9999*ones(86400,1);
PPN_final = -9999*ones(86400,1);
MPAN_final = -9999*ones(86400,1);

for x = 1:length(Days_July{z});
  time_stamp = Days_July{z}(x,5);
  location = find(utc_seconds == time_stamp);
  PAN_final(location) = Days_July{z}(x,7);
  PPN_final(location) = Days_July{z}(x,8);
  MPAN_final(location) = Days_July{z}(x,9);
end

final_file = [utc_seconds, PAN_final, PPN_final, MPAN_final];
day_of_month = num2str(z+7); % data for July starts on the 9th
name = ['BAO_PAN_PPN_July_' day_of_month '_2014_RB.csv'];
csvwrite(name,final_file);

end

for z = 1:22; % Data for BAO goes to August 22nd
PAN_final = -9999*ones(86400,1);
PPN_final = -9999*ones(86400,1);
MPAN_final = -9999*ones(86400,1);

for x = 1:length(Days_August{z});
  time_stamp = Days_August{z}(x,5);
  location = find(utc_seconds == time_stamp);
```

```
  PAN_final(location) = Days_August{z}(x,7);
  PPN_final(location) = Days_August{z}(x,8);
  MPAN_final(location) = Days_August{z}(x,9);
end

final_file = [utc_seconds, PAN_final, PPN_final, MPAN_final];
day_of_month = num2str(z);
name = ['BAO_PAN_PPN_August_' day_of_month '_2014_RB.csv'];
csvwrite(name,final_file);

end
```

The MatLab code takes the .csv file mentioned above and outputs a .csv file for each day of the campaign. The code converts the raw peak areas into pptv, eliminates in situ calibrations, and outputs data at 1 Hz frequency (giving a lot of NaNs). The .csv files are named according to the following convention: “BAO_PAN_PPN_Month_dayofmonth_2014_RB.csv” The files are only missing the headers for the ICARTT convention. Emily Fischer created the final ICARTT files.